Title: Fear and foraging opportunities interact with temperature and seasonality to drive diversity in fish life histories

Running Title: Ecosystem size spectra drive life history diversity

Authors:
Kindsvater, Holly K.[1], Juan-Jordá, Maria-José[2,3], Dulvy, Nicholas K.[2], Horswill, Cat[4,5,6], Matthiopoulos, Jason[7], Mangel, Marc[8,9]

1. Dept. of Fish and Wildlife Conservation, Virginia Polytechnic Institute and State University, 310 W. Campus Dr., Blacksburg, VA 24061, USA
2. Earth to Ocean Research Group, Dept. of Biological Sciences, Simon Fraser University, Burnaby, BC V5A 1S6 Canada
3. AZTI Tecnalia, Herrera Kaia, Gipuzkoa, Spain
4. ZSL Institute of Zoology, Regent's Park, London, NW1 4RY, UK
5. Centre for Biodiversity and Environmental Research, Department of Genetics, Evolution and Environment, University College London, Gower Street, London, WC1E 6BT, UK
6. Department of Zoology, University of Cambridge, Downing St, Cambridge CB2 3EJ, UK
7. Institute of Biodiversity, Animal Health and Comparative Medicine, Graham Kerr Building, University of Glasgow, Glasgow, G12 8QQ, Scotland.
8. Theoretical Ecology Group, Dept. of Biology, University of Bergen, Bergen 5020, Norway
9. Institute of Marine Sciences and Dept. of Applied Mathematics and Statistics, University of California, Santa Cruz, CA 95064, USA.

Keywords – Body size evolution, ecosystem size spectra. climate change, metabolic theory, state-dependent models

Abstract

Understanding how fish growth and reproduction will adapt to changing environmental conditions is a fundamental question in evolutionary ecology. Analyses of the physiological effects of climate change upon life histories and population demography rarely consider size-dependent foraging and risk of predation. We embedded a state-dependent energetic model in an ecosystem size spectrum to model prey availability (foraging) and risk of predation (fear) experienced by individual fish as they grow. We predicted emergent body sizes and reproductive and mortality patterns in the context of ecosystem food web interactions, represented by size spectra. We found that more productive spectra led to larger body sizes, but effects of temperature on body size were relatively small. We applied our model to abiotic scenarios corresponding to species representing the three ecological lifestyles (ecotypes) of tunas, considering environments that included seasonal variation in temperature. We predicted realistic patterns of growth of all tuna ecotypes. Unexpectedly, we found that individuals grew larger when they experienced higher productivity or colder temperatures for part of the year. This increase in body size emerged because spawning opportunities were constrained to part of the year, and explained the evolution of gigantism in temperate tunas. Our framework for predicting emergent life histories combines direct and indirect effects of productivity (foodscapes), individual risk (fearscapes), and metabolic processes and offers a promising approach to understand fish life history responses to changing ocean conditions.

Introduction

The body sizes and population biomasses of aquatic species are changing rapidly to human-induced environmental change (Oke et al. 2020), motivating the need for biophysical models to predict growth and reproduction in changing environmental conditions (Cheung et al. 2008, Cheung et al. 2010, Blanchard et al. 2012, Fernandes et al. 2020). Beyond thermal physiology, the evolutionary consequences resulting from changing ecosystem productivity (foodscapes) and predator abundance (fearscapes) are difficult to disentangle from the effects of changes in prey field richness, predation risk or seasonality on growth and related life history traits (Daufresne et al. 2009, Audzijonyte and Richards 2018, Neubauer and Andersen 2019). Classic and recent advances predicting optimal growth and reproduction of harvested populations (Holt 1958; Beverton and Holt 1959; White et al. 2022) have been combined with size-structured community interactions to predict the evolution of life history traits in specific taxa (Shuter et al. 2016). This approach provides a promising foundation for predicting ecological and evolutionary responses to climate change. While specific taxa within an ecosystem will adapt according to contextual factors such as phylogenetic lineage, adaptive capacity, and environmental variability, models incorporating the roles of food and fearscapes, seasonality, and other metabolic processes could explain adaptive variation among closely related taxa and refine our mechanistic understanding of species' responses to changing climate conditions (Free et al. 2019). By examining closely related species that have invaded different environments, such as the market tunas (Scombridae), we can gain insight into how physiological adaptations to thermal conditions, productivity (prey richness) and seasonality affect allocation to growth and reproduction. This can help move us beyond broad macro-ecological patterns toward a more mechanistic understanding of the

mechanisms underlying existing diversity and improve predictions of responses to future change (Alvarez-Noriega et a. 2023).

In ectothermic species with indeterminate growth, including fish, food availability and risk of predation both increase as individuals grow larger, and growth rates can be selected to be slower or faster depending on the size-dependence of per-capita resource availability and predication risk (Conover and Munch 2002; Walsh and Reznick 2009, Hulthén et al 2021). At the same time, development at higher temperatures can lead to smaller body sizes, within and between ectothermic species (Kingsolver and Huey 2008). Trade-offs among these life-history traits determine individual body sizes and population demographic rates (Beverton and Holt 1959, Gadgil and Bossert 1970, Kozlowski 1992, Kozlowski 1996), but existing theory struggles to predict how ontogenetic increases in prey availability and decreases in predation risk with size, along with interacting effects of temperature and seasonality, affect the evolution of growth (Varpe 2017). There is longstanding interest in the mechanisms leading to biphasic or asymptotic growth patterns (Quince et al. 2008). The earliest growth models, including the von Bertalanffy growth model, were based on hypothesized differences in the allometric scaling of anabolism (resources taken in) and catabolism (resources spent) (von Bertalanffy 1960, Audzijonyte et al. 2022). Such growth models are routinely fit to data on size-at-age of fishes, but their mechanistic justification is necessarily simplistic; such models struggle to explain latitudinal and temporal trends in body size within and among species of fish (Audzijonyte et al. 2020), suggesting that they do not sufficiently capture the relevant intrinsic physiological and extrinsic ecological drivers of fish life histories.

The role of metabolic requirements and the trade-off between growth and reproduction has shaping growth trajectories has been given increasing attention in recent decades (Jørgensen et al. 2016, Wong et al. 2021, White et al 2022). Physiological processes can vary with the environmental temperature experienced by organisms (Brown et al, 2004, Clarke and Johnston, 1999). The allometric scaling of metabolic costs in different temperature regimes (known as the Metabolic Theory of Ecology [MTE]; Gillooly et al. 2001) has been used to predict individual body size according to the benefits of growing large (to increase foraging success and avoid predation), balanced against the costs of increased metabolic overhead and diverting resources from reproduction to growth (Wong et al. 2021). More detailed models of energetic allocation have linked variable environmental conditions to growth, reproduction, and longevity (Kozłowski and Teriokhin 1999, Cichoń and Kozłowski, 2000, Lika and Kooijman 2003, Jorgensen and Fiksen 2006, Audzijonyte et al. 2022). Understandably, the results of these models depend on specific assumptions regarding mass-based foraging success and risk of predation.

To predict growth when individuals experience mass-dependent resource availability and predation risk in environments of differing temperatures, productivity, and seasonality, we draw on ecosystem size-spectra theory to reduce the number of *ad hoc* assumptions required about the scaling of these ecological processes, which arise from community interactions. We hypothesize this approach could yield more realistic predictions of diversity in fish life histories, providing significant insights into the mechanisms that determine adaptive responses to changing environmental conditions. In aquatic ecosystems, size spectra are an emergent property of community interactions (Sheldon et al. 1977, Thygesen et al. 2005, Law et al. 2009, Sprules and

Barth 2016, Christensen and Andersen 2011, Andersen et al. 2016, Andersen 2019). In a community size spectrum, flow of energy between trophic levels via consumption and predation rates are characterized by individual mass, instead of species' identity (Benoît and Rochet 2004, Blanchard et al. 2009, Andersen 2019). The key property of size spectra is that an individual's relative position (mass) determines both its prey field (foodscape – or the area under the size spectrum to the left of an individual's mass) and its risk of predation (fearscape – the area to the right). Individuals are born small and grow through the size spectrum over their lifetime, consuming prey that are a fraction of their own size. Furthermore, size-spectrum theory assumes the lower limit of prey size preference depends on the profitability of the prey, and any upper limit depends on the maximum gape size of the predator. These interactions could equally apply to interactions within size-structured populations of the same species (i.e., cannibalism). Therefore, predation and consumption rates determined by different areas under a size-spectrum curve could be used to simultaneously characterize the mass-specific caloric resource availability and risk of predation experienced by an individual as it grows (Benoît and Rochet 2004, Giacomini et al. 2013, Shuter et al. 2016, Andersen 2019).

Here, we use an energy-based model combining size-dependent resources and risk of predation (both derived from size-spectra) with size- and temperature-dependent physiological requirements predicting the evolution of growth, maximum body size, reproductive investment, and longevity in different environments. We define fitness as expected lifetime reproductive success and determine its maximum value and the associated life history decisions (allocation to maintenance, growth and reproduction) using stochastic dynamic programming (Clark and Mangel, 2000, Houston et al.1988, Mangel, 2015). Within this extended framework, we examine

general patterns in the life history evolution of fishes under different scenarios of ecosystem productivity and environmental temperature.

We next investigate the evolution of growth, body sizes and reproductive patterns in tuna species in varying environments, including seasonally varying conditions. Tunas (Family *Scombridae*) exhibit a wide range of maximum body sizes (~ 40 cm - 400 cm), longevities (~ 4 - 41 years) and reproductive patterns (Juan-Jorda et al. 2013, Horswill et al. 2019). Tunas are epipelagic species found in temperate and tropical waters around the world's oceans with varying vertical, latitudinal and seasonal distributions and movements. Confronting the predictions of our model with data on the life history diversity observed in tuna species in different environmental conditions gives us insight into the mechanisms underlying fish life histories and improve our ability to predict their response to future climate scenarios. Where possible, we use values for physiological processes measured for tunas, but we also consider the sensitivity of our results to these parameters to ensure their generality.

Methods

Using the size spectrum to infer mass-specific rates of prey encounter and predation

The relationship between the numbers of organisms and individual mass w is a power function with a scaling parameter κ and an exponent λ, which has been empirically estimated to be close to -1 such that abundance is inversely proportional to mass (Sheldon et al. 1972, Trebilco et al. 2013, Sprules and Barth 2016, Hatton et al. 2021)

$$N(w) = \kappa w^{\lambda} \tag{1}$$

The Sheldon size spectrum, which follows from Eq. 1, is the distribution of total ecosystem biomass *B(w)* across body size classes, and is represented by $B(w) = N(w)w$. Based on evidence from multiple ecosystems (Sprules and Barth 2016), the spectrum – as originally conceived (Sheldon et al 1972) and recently confirmed (Hatton et al. 2021) – is nearly flat, or may very slowly decrease as body size increases. Since $N(1) = \kappa$, we view κ as a metric of ecosystem productivity. In a log-log plot of Eq. 1, the intercept is the natural log of κ.

This phenomenon of linear aquatic size spectra emerges from three size-dependent processes: (1) the encounter rate of predators and prey; (2) the preference of predators for prey of a given size; and (3) the limit to prey consumption imposed by the size of the predator's stomach (the predator-prey mass ratio; Benoît and Rochet 2004, Blanchard et al. 2017, Andersen 2019). Anderson (2019) derived a method to calculate the prey available to individuals of mass *w* by relating the productivity of a spectrum to empirical estimates of prey encounter rates, predator-prey mass ratios, and prey preferences. Following his rationale, we assume that the prey biomass available per month to an individual is a concave function of mass *w*, and scaled to be approximately three times the size spectrum productivity κ (Andersen 2019). The empirical estimates of physiological processes used to simplify this derivation are associated with a significant amount of variability among species within a size class (Andersen 2019). Following Andersen, as a baseline the per-period food available for an individual of mass *w* is represented by

$$B_{prey}(w) = 3\kappa w^{0.05} \tag{2}$$

This equation approximates the integral over the foodscape of prey biomass (in kg) available to an individual of mass *w* each month (Fig. 1A), and includes a threefold scaling factor from empirical analyses (Andersen 2019). The foodscape is therefore the total biomass available to the predator, and the range of sizes of prey that it takes. To address variability across ecosystems in productivity, we chose to vary κ in subsequent analyses, representing potential differences among taxa or other ecosystem processes.

We define the fearscape as an individuals' instantaneous risk of predation, integrated across sizes of potential predators. For gape-limited taxa like fishes, a predator's prey field depends on its encounter rate with prey in its preferred size range. This encounter rate (the clearance rate) is typically measured in units of volume per time, as aquatic species forage in a three-dimensional habitat (Kiørboe and Hirst 2014). Again, we follow Andersen (2019), and in Eq. 3 (defined below) we use an empirically estimated constant of 0.07 to characterize the scaling of prey vulnerability with its mass, which is based on estimates of preference windows of predators and the volume of water each clears per month that come from empirical distributions of prey sizes in predator guts (Ursin 1973). We also define a coefficient *h,* which modifies the probability of consumption - how likely a predator is to capture the focal individual (based on its hunger level or capture efficiency) - and use the reported allometric exponent of -0.25 to represent how predation mortality scales with body size (Figure 1B; Eq. 2.22 in Andersen 2019). From these, Anderson (2019) integrates over the Sheldon spectrum and produces a relationship predicting the scaling of mortality risk for prey $\mu_p(w)$ per month:

$$\mu_p(w) = 0.07hw^{-0.25} \tag{3}$$

We convert this instantaneous rate to the probability of escaping from predators during each time interval (Hilborn and Mangel 1997, Mangel 2006), so we can represent the probability an individual survives $\gamma_{pred}(w)$ as:

$$\gamma_{pred}(w) = e^{-\mu_p(w)} \tag{4}$$

The resulting mass-specific survival through each month is is plotted for different values of *h* in Fig. 1B.

Defining physiological costs that depend on temperature and body mass

We assume metabolic costs that increase with body mass and environmental temperature (Clarke 2006). We model individual costs $C(w, \tau)$ (in joules) as a function of temperature τ in Kelvin, following the general form introduced in the MTE (Gillooly et al. 2001):

$$C(w, \tau) = cw^{\theta} e^{\left(-E/k_B\tau\right)} \tag{5}$$

Evidence for the MTE suggests the activation energy *E* (the energy required for the reactions of respiration and other metabolic processes) does not vary appreciably among taxa (Bernhardt et al. 2018); Boltzmann's constant k_B also does not vary. The normalization coefficient *c* accounts for differences among taxonomic groups in the intercepts of the linear relationship that arise from second-order effects such as stoichiometry or respiratory surface areas (Bigman et al 2021). The slope of this relationship in log space, θ, is strikingly similar among taxa (Brown et al.

236 2004). We use a value for θ estimated from physiological studies on tunas (Table 1) but vary it in
237 sensitivity analyses. Note that τ in Eq. 5 is traditionally in Kelvin. However, we rescale all
238 values in our results in units of Celsius. We use this general formula for scaling of metabolic
239 costs at different temperatures τ to describe the monthly energetic expenses of an individual of
240 mass w (Fig 1C). Defining the relationships in Eqs. 2, 4, and 5 allowing us to specify mass-
241 dependent survival and energy dynamics and therefore examine the variables influencing growth
242 and reproduction in a common currency of individual fitness. All parameters are defined and
243 their values reported in Table 1.

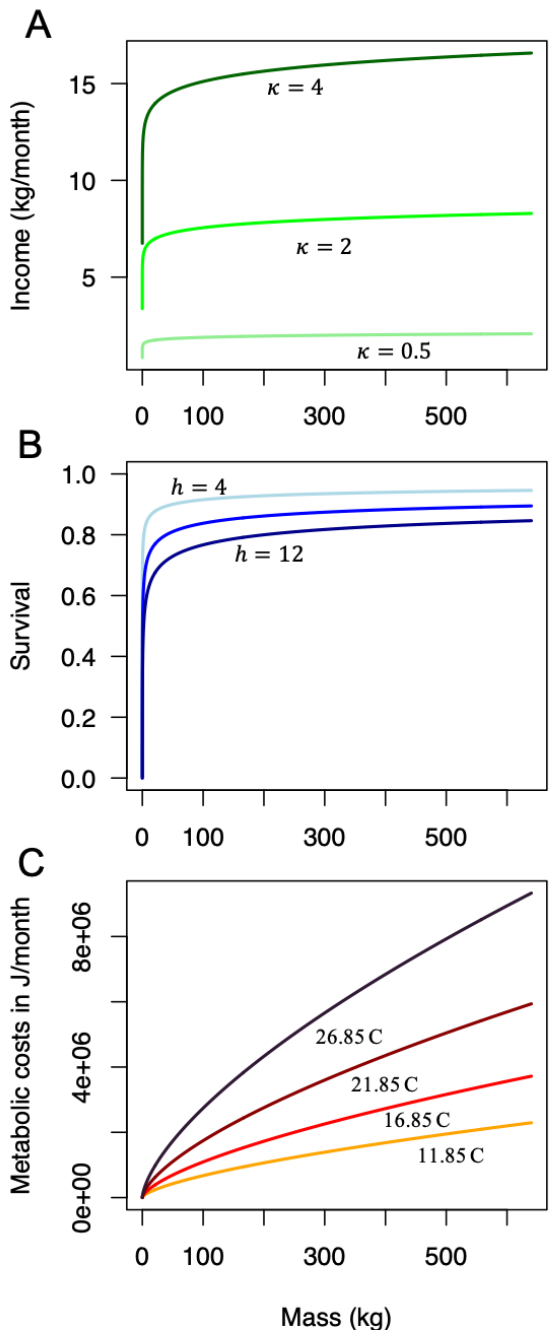

Figure 1. Examples of allometric relationships between individual mass and (A) income (in kg per month) for differing ecosystem productivities κ (Eq. 2); (B) the scaling of survival with size and its interaction with predator efficiency (or hunger) h (Eq. 4), and (C) metabolic costs (Eq. 5), which also scale with temperature τ (on the graph, it is presented in degrees Celsius, °C; values in Kelvin are 285, 290, 295 and 300K). Note that these curves represent a subset of values considered.

Defining fitness and determining the optimal allocation strategy

To find the optimal life history strategy in different scenarios of ecosystem productivity and temperature conditions, including seasonal variation, we developed a model of an individual's energy budget, tracking two physiological state variables, the body length l and energy (lipid) stores s of an individual, which vary dynamically over an individual's lifetime (Fig. 2). Following the conventions for dynamic state-variable models, we denote the state variables l and s are lowercase in the dynamic programming equation, representing the fact they are iterated values. Later, when we refer to specific values of the state variables, we use uppercase L and S.

We define fitness as expected lifetime reproduction, averaged over the stochastic process of survival, which we calculate numerically using stochastic dynamic programming (Houston et al. 1988; Clark and Mangel 2000, Mangel, 2015). This method allows us to consider how individual age and physiological state (energy stores and body length) affect the optimal trade-off between growth and reproduction in the context of lifetime fitness. We assume that an individual allocates a proportion of its budget to growth and reproduction on monthly time intervals. Our choice to model allocation to growth and reproduction as proportions of an individual's energy budget builds on prior dynamic state-variable models of fish growth (Jørgensen and Fiksen 2006, Chapman et al. 2011).

Given specific values of $L(t)$ and $S(t)$, representing individual length and energy stores at the start of month t, we calculate structural mass $W(t)$ from length with a standard cubic function (Froese 2006):

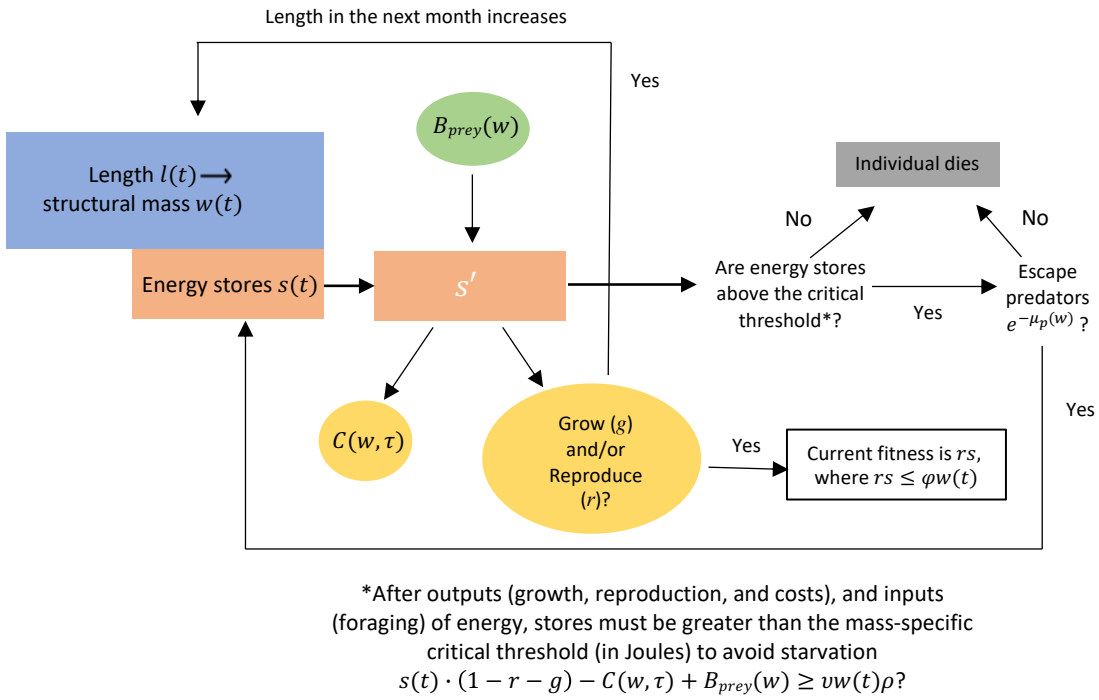

Figure 2. Conceptual overview of the optimization algorithm calculating the two dynamically varying state variables, body length $l(t)$ and energy stores $s(t)$ within each month t, as well as current and expected fitness. Arrows represent the flow of energy or decisions. Round shapes represent energetic input (green) and outputs (yellow); rectangular shapes are model states and outputs (fitness and fate). Note that $l(t)$ and $w(t)$ are related through Eq. 6. Both B_{prey} and μ_p are determined by the size spectrum.

Given specific values of $L(t)$ and $S(t)$, representing individual length and energy stores at the start of month t, we calculate structural mass $W(t)$ from length with a standard cubic function (Froese 2006):

$$W(t) = aL(t)^3 \tag{6}$$

and assume that only structural mass is relevant for size-dependent gains (B_{prey}) and costs (Fig. 2). We convert from mass to units of energy (joules) and back using a conversion factor estimated for tunas ($\rho = 4.2 \times 10^6$J/kg; Chapman et al 2011) but that could take other values for other species. Each month, an individual acquires energy from food, determined by their structural mass *w* via Eq. 2. We then allow the individual to allocate proportions of its energy budget (which includes income and any stored energy) to growth (*g*) and reproduction (*r*). Given an individual with specific values for length $L(t)$ and energy stores $S(t)$, we calculate the increment of growth expected for each possible proportional allocation *g* by converting the fraction of lipid stores from joules to the equivalent mass ($g\frac{S(t)}{\rho}$), and then adding it to existing mass, such that $W(t+1) = W(t) + g\frac{S(t)}{\rho}$. We then calculate the new length by rearranging the mass-length relationship $W(t) = aL(t)^3$:

$$L(t+1) = \left(L(t)^3 + g\frac{S(t)}{a\rho}\right)^{1/3} \tag{7}$$

We repeat this for every possible combination of values of the state variables, *l* and *s*. Values for proportional allocation of lipid stores to reproduction *r*, along with *g*, are combined to determine the dynamics of energy stores and length from one month to the next:

$$S(t+1) = B_{prey}(W(t)) - C(W(t),\tau) - (r+g)\cdot S(t) \tag{8}$$

We assume that both stored energy and reproduction are limited by an individual's structural mass (which in turn depends on its length). These constraints represent limits on the amount of

lipid that it is realistic to store, and mass of gametes that can be produced, given the capacity of the body cavity. If the proportions of energy allocated to reproduction and growth are less than 100% (meaning $r + g < 1$), the remaining energy is stored for future use, as long as total reserves do not exceed 60% of structural mass. This value is arbitrary but exploratory analyses suggest it does not have a strong effect on the results presented here because in practice individuals do not store their energy long enough to come close to exceeding this limit. Second, we assume that reproductive output (in units of kg) is constrained so that it cannot exceed a fixed proportion of φ of structural mass $w(t)$, so that the following condition must be met:

$$\frac{rS(t)}{\rho} \leq \varphi w(l,t) \tag{9}$$

This size-based limit on total reproduction is used in the calculation of current fitness.

Expected future fitness

At any age, expected fitness is determined by the sum of current reproduction and accumulated future reproduction, which is calculated assuming the individual behaves optimally at all future ages. This requires we calculate the future states (length and lipid stores) given each combination of allocation to growth and reproduction. We denote potential values of future states as $l'$and s'. These are

$$l'(l,s,g) = l + \left(l(t)^3 + g\frac{s}{a\rho}\right)^{1/3}$$

$$s'(l,s,r,g) = B_{prey}\big(w(l)\big) - C(\,w(l),\tau) - (r+g)s \tag{10}$$

where $w(l)$ is the structural mass of an individual of length l. At the end of the month, if an individual's lipid stores fall below the critical threshold for its mass (its expenditures have exceeded its energy budget), it starves (Supp. Fig. 2). We let $\gamma_s(s,l)$ denote the probability of avoiding starvation in the current time and model it as

$$\gamma_s(s,l) = \frac{1}{1+e^{-q(s-\upsilon w(l)\rho)}} \tag{11}$$

involving two new parameters υ and q. The parameter υ determines the level of stores at which starvation begins and q is a shape parameter. When $s = \upsilon w(l)\rho$, the right-hand side of Eq. 11 is always ½. When q is large, then the right-hand side of Eq. 11 is approximately one when $s > \upsilon w(l)\rho$ and zero otherwise. Thus, this function specifies that if combined allocation to growth and reproduction causes an individual's lipid stores to decrease below the critical value for its mass the probability of survival decreases smoothly toward zero (See Supp. Fig. 1 for more details).

Equations 7-11 characterize changes in individual state and in fitness, given the possible monthly allocation strategies (r and s). With these functions in place, we can find the allocation strategy that maximizes current and future fitness at every age until the age of senescence or maximum lifespan, T, is reached (for all scenarios, we assumed the maximum lifespan of T = 216 months or 18 years). We define $V(l,s,t)$ as the maximum expected accumulated reproduction between time t and T, given size $L(t) = l$ and lipid stores $S(t) = s$. Since there can be no

accumulated reproduction after *T,* we have the end condition $V(l, s, T) = 0$. Expected future fitness at every age $t < T$ is found by solving the stochastic dynamic programming equation

$$V(l, s, t+1) = \max_{g,r}\left[R(r, l, s, t) + \gamma_{pred}(w) \cdot \gamma_s(s, l) \cdot V\big((l'(l, s, g), s'(l, s, r, g), t\big)\right] \qquad (12)$$

The first term of the on the right-hand side of Eq. 12 represents reproduction in month *t*. The second term represents expected future reproduction, discounted by the probability of surviving predation $\gamma_{pred}\ (w)$ and starvation $\gamma_s(s, l)$, When these are combined, we obtain expected lifetime reproduction from time *t* onwards, given that size $L(t) = l$ and lipid stores $S(t) = s$.

The dynamic programming algorithm (Mangel and Clark 1988; Houston and MacNamara 1999) iterates over all viable combinations of *l* and *s,* at each time *t,* and stores the fitness of each allocation strategy. The optimal strategy (marked with an asterisk) at time *t* is the combination g^* and r^* associated with the greatest current and future fitness. Further details of the optimization algorithm are given in the Appendix. In Supp. Fig 3 we illustrate the array for both allocation strategies (*g*(l,s,t)* and *r*(l,s,t)*) at two ages, for all possible combinations of length and lipid stores.

Calculating the fate of individuals allocating optimally

We used a Monte Carlo simulation to calculate the accumulating probability of mortality as an individual ages, following the allocation rules generated by the solution of Eq. 12, which provides optimal allocation rules for the range of state values specified in our numerical algorithm. Some combinations of states (length, lipid stores and age) will not arise naturally and

367 others are inviable (the dark blue regions of Supp. Fig. 3). Therefore, to predict the relationships
368 between length, lipid stores, and age that will be observed in nature, we simulate the expected
369 fates of an individual that is born at a given size, and allocates energy according to the optimal
370 growth and reproduction fractions given by the solution to Eq. 12. We record the body length
371 and reproductive output in each subsequent month of an individual's life, and calculate its
372 probability of survival, given both the risk of starvation and the risk of predation. The expected
373 lifespan was defined as the age past which the cumulative chance of survival is less than 3%,
374 which we use as an arbitrary definition of lifespan. For simplicity, we consider reproductive
375 output in units of energy (joules) rather than considering allocation to offspring size and number
376 (Kindsvater et al. 2010); this can include migration costs. We did not build in any assumptions
377 about age at maturation, but rather let maturation patterns, along with natural trade-offs between
378 growth and reproduction (Supp. Fig. 3) emerge from patterns of allocation.
379
380 *Scenarios for environmental variation*
381 We used our model to predict a range of fish life histories (growth, reproduction, and survival)
382 that are evolutionarily advantageous across different scenarios of ecosystem productivity and
383 environmental temperatures. To do this, we developed different productivity and temperature
384 scenarios corresponding to different conditions in the marine environment and impose different
385 metabolic costs to individuals according to Eq. 5. We solved for the optimal life histories under
386 different temperatures (τ in Eq. 5 in units of Kelvin), converted to Celsius and ranging from
387 11.85 to 26.85 ℃ (285-300 K) in five-degree intervals. We considered these temperature ranges
388 in different scenarios for ecosystem productivity, for which κ ranged from one to five. We

389 considered factorial combinations of these parameters to understand the implications of their
390 interactions for the evolution of fish life histories.
391
392 *Case study predicting life history diversity of tunas (Scombridae).*
393 We developed a case study for tunas to examine if our model can predict the general patterns of
394 life history variation in tunas. There are 15 species of tunas within the Family *Scombridae*, from
395 five genera *Allothunnus*, *Auxis*, *Euthynnus*, *Katsuwonus*, and *Thunnus*. These species inhabit a
396 wide range of environmental conditions in marine ecosystems. Tunas can be found in coastal and
397 oceanic pelagic waters, and have wide geographic distributions, ranging from the tropics to
398 higher temperate latitudes with some degree of habitat partitioning by depth. Tropical tunas can
399 spawn throughout the year, while the subtropical and temperate tunas undergo seasonal
400 migrations returning form cool high latitude feeding grounds back to warm waters for spawning
401 (Juan-Jordá et al 2013, Horswill et al 2019). Paleoceanographic evidence suggests that ancestral
402 tunas evolved in a tropical environment approximately 60 million years ago (Monsch 2000) and
403 over time they have diversified and evolved a suite of morphological and physiological
404 adaptations that have allowed them to expand their distributions into more temperate
405 environments or deeper colder waters where they can encounter higher prey densities to support
406 their high somatic and gonadal growth rates (Dickson and Graham 2004). Reflecting their
407 tropical ancestor, all tunas (except for the slender tuna *Allothunnus fallai*) spawn in warm waters,
408 requiring a sea surface temperature of at least 24 ℃ (Schaefer 2001). This is a key aspect of their
409 reproductive biology that we include in our model scenarios.
410

411 To connect our mechanistic model more explicitly with the observed patterns of life history
412 variation in tunas, we followed a proposed categorization of tunas into three ecological lifestyles,
413 (Bernal et al. 2017). The three general lifestyles are based on species-specific vertical,
414 latitudinal, and temporal (seasonal) distributions and movement patterns of tunas (Figure 3;
415 Bernal et al. 2009, Bernal 2011, Bernal et al. 2017). The first ecological lifestyle represents a
416 tuna species that largely remains within the warmer and well-oxygenated surface layer above the
417 thermocline (generally above 20 °C) during both day and night. These tuna species have limited
418 vertical movements as they do not descend below the thermocline (Figure 3). Coastal species,
419 such as the tropical frigate tuna (*Auxis thazard*) may typify this group. The second ecological
420 lifestyle represents tuna species that spend the majority of the time above the thermocline
421 (generally above 20 °C) but also visit depths below the thermocline for foraging (Figure 4). The
422 oceanic species of yellowfin tuna (*Thunnus albacares*) with year-round tropical distributions
423 typifies this group. Its vertical movement exposes this species to a wider range of temperatures
424 and to less-oxygenated waters at depth but only for short periods of time because this species is
425 not hypoxia tolerant (Schaefer et al. 2009). The third ecological lifestyle characterizes tuna
426 species that are exposed to a wider range of environmental conditions and spend significant
427 periods of time in colder waters (Figure 3). The oceanic and temperate Atlantic bluefin tuna

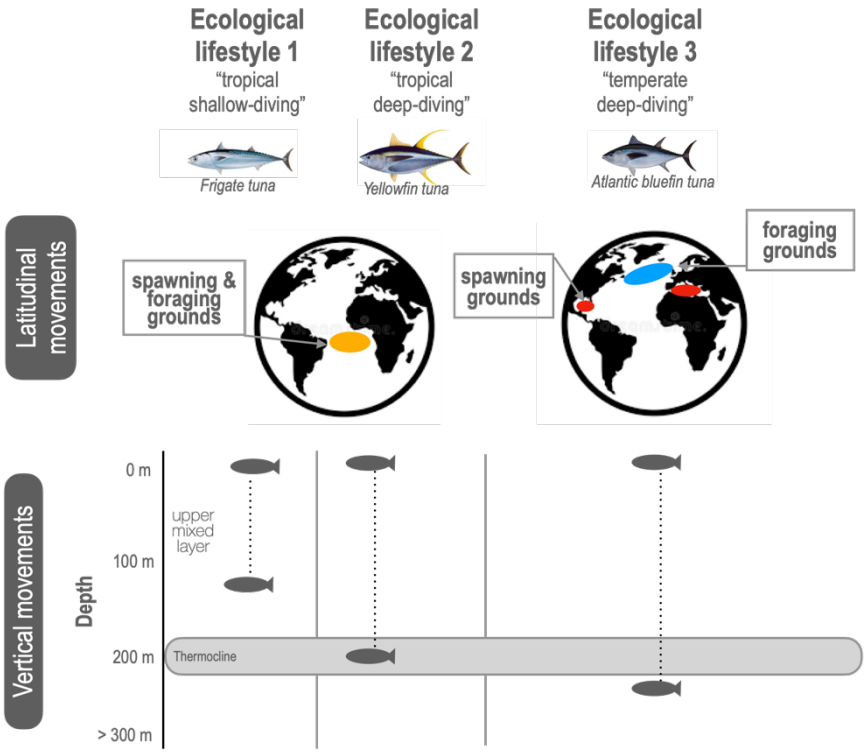

Figure 3. Three representative ecological lifestyles of tunas and their distribution patterns based on their latitudinal and vertical movements. Characteristic spawning and foraging grounds are shown for each lifestyle; examples are the tropical shallow-diving frigate tuna *Auxis thazard*, tropical deep-diving yellowfin tuna *Thunnus albacares,* and temperate deep-diving Atlantic bluefin tuna *Thunnus thynnus*. Fish silhouettes represent the depth distribution where species spend most of their time. The thermocline is defined as the depth range within which the water temperature changes rapidly and separates the water column into the upper well-mixed surface layer (water above 20 °C) and the deeper waters (waters below 15 °C). Figure modified from Bernal et al. 2009 and Bernal et al 2017.

428 (*Thunnus thynnus*) are one species that typifies this group, spending most of the year at higher
429 latitudes in colder and more productive waters between the upper mixed later and the cooler deep

waters below the thermocline, and migrating to warmer waters for spawning (Bernal et al. 2017).

To examine whether our model could predict these three broad ecological lifestyles of tunas, we modelled environmental scenarios corresponding to each lifestyle in terms of temperature, ecosystem productivity, and seasonality. We chose parameters based on the results of our general model, but also added seasonal fluctuations in temperature to represent the bluefin tuna migration from temperate, productive waters to their tropical spawning grounds. We then asked whether the traits emerging in these scenarios matched the range of reported sizes of three representative species corresponding to each lifestyle (Juan-Jordá et al. 2016).

Sensitivity analyses

We ran a series of tests to examine how our choices of parameters in the size spectrum influence model predictions. Specifically, we varied values of h (representing efficiency in prey capture or hunger levels) in the predation function (Eq. 3) and φ (the fraction of body mass that can be devoted to reproduction) in the reproductive constraint (Eq. 9). We also conducted sensitivity analyses in which we varied the scale and shape coefficients in the metabolic cost function (c and θ, respectively, in Eq. 5). Motivated by our tuna case study, we also varied seasonality in resources, temperature, and spawning. We considered seasonal environments in which only resources and only temperature varied, to understand how these factors alone contributed to observed variation in body size and reproductive output. We additionally considered growth and reproductive patterns with an expanded the warm season (where individuals could spawn in warm temperatures for six months of the year, instead of three). Finally, we determined in

preliminary analyses that the maximum lifespan T did not strongly affect model results, because most individuals reach a maximum body size well before the final time T.

Results

An asymptotic growth pattern naturally emerged from the model, after a period of exponential growth early in life (Fig. 4). Our model predicted age-specific relationships between body size (length, from which we calculate mass using Eq. 6) and reproduction that correspond to a range of fish life histories (Fig 4). In general, we found that individuals allocated energy to growth early in life and shifted this allocation to reproduction in later life. Ecosystem productivity (κ) alone generated a range of maximum body sizes, from less than 100 cm at low levels of productivity to well over 350 cm (Fig. 4A). Across scenarios of ecosystem productivity, the predicted trajectories for individual growth were identical in early life. However, growth slowed earlier in lower productivity environments (Fig. 4A). For all life histories, allocation to reproduction began at very low levels sometime during the individual's second year (Fig. 4B) and increased steadily as the individual aged. Both the rate at which reproduction increased with size and the maximum reproductive output were consistently greater with increased ecosystem productivity (Fig. 4B). We also found the pattern of age-specific mortality was very similar in early life for all productivities κ, but that lifespan increased predictably as asymptotic body size increased (Supp. Fig. 5).

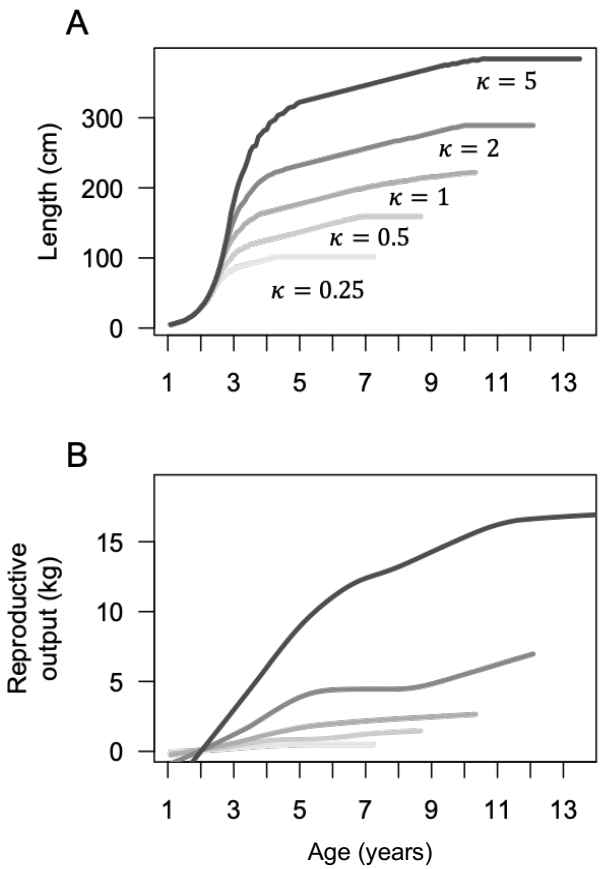

Figure 4. (A) Growth (length at age) and (B) Expected reproductive output of individuals in different productivity κ scenarios. Each curve ends when an individual's expected survival chances are less than 3%. Temperature in every scenario was constant at 16.85 ℃, and h was constant at 8. The reproductive output was smoothed using the loess tool in R; data points can be found in Supp. Fig. 4.

When we compared the interacting effects of ecosystem productivity (κ) and environmental temperature (τ) on patterns of growth and reproductive allocation, we found the effects of temperature on body size and reproductive output were relatively small (Fig. 5). The biggest differences emerged in highly productive environments with dramatic increases in temperature. Specifically, when average temperature increased by 10 degrees (e.g., from 11.85 to 21.85 ℃ or from 16.85 to 26.85 ℃), maximum body sizes were 3-10% smaller, with the largest differences occurring when $\kappa = 5$ (specific values in Fig. 5 are reported in Supp. Table 1). At the same time, these increases in temperature led to concomitant reductions in lifetime reproductive output that ranged from 3-10% (Fig 5B). However, it is important to note that comparing thermal increases

481 in 5-degree intervals only generated minor (3-5%) decreases in growth and reproduction, unless

482 both predators and prey were scarce ($\kappa \leq 0.5$, Supp. Table 1).

483

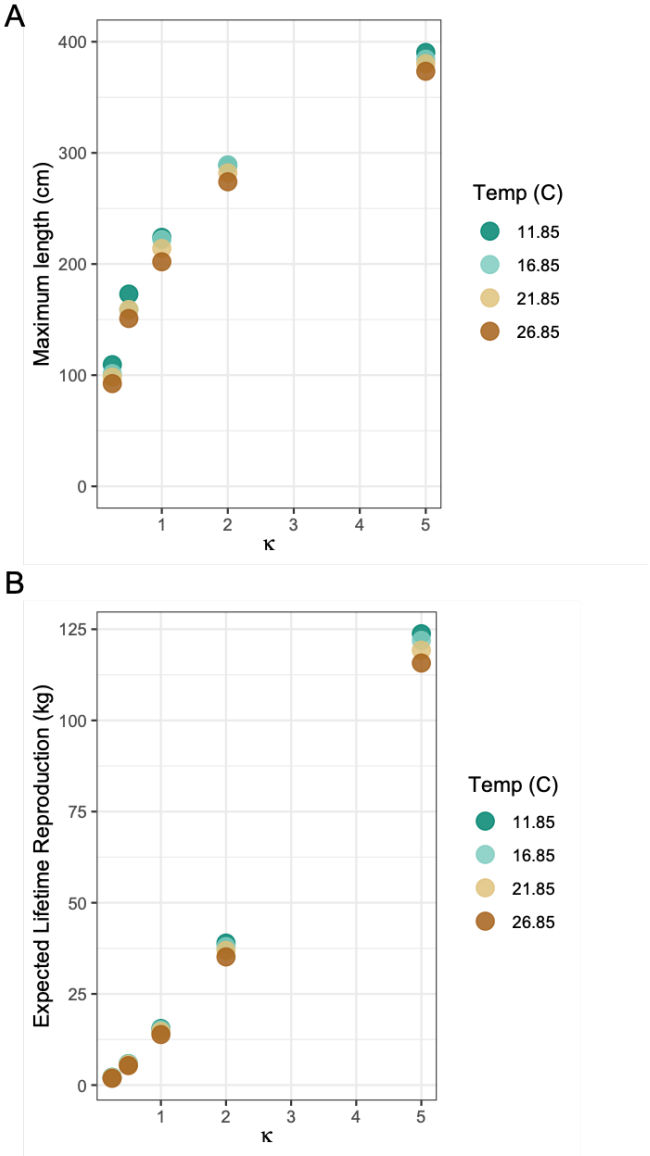

Figure 5. (A) Maximum body size and (B) Expected lifetime reproductive output (in kg) of individuals plotted against a range of productivity scenarios. Color of points corresponds to differences in average annual temperature in °C.

484

485 The interacting effects of temperature and productivity on body size suggests that when both

486 prey and predators are abundant, the benefits of growing large outweigh associated increases in

487 metabolic costs. Remaining smaller in thermally taxing conditions (to minimize energetic

488 requirements for maintenance), equates to an increased risk of predation and thus shorter

489 lifespans. In other words, the effect of temperature on survival was indirectly expressed through
490 body size, i.e., where temperature influenced asymptotic body size (Fig. 5A) it had a predictable
491 effect on lifespan.
492
493 To understand the robustness of the main result in Fig. 5, we conducted sensitivity analyses. We
494 varied the parameter *h,* representing predator efficiency or hunger level (Eq. 3; Andersen 2019),
495 to change the allometric properties of the risk of predation (Supp. Fig. 6). However, while
496 varying this parameter affected the realized lifespans, it did not dramatically change individual
497 growth trajectories or patterns of size-specific reproduction (Supp. Fig. 6). By contrast, the
498 constraint on the amount of lipid stores that can be spent each month on reproduction, φ, was of
499 more importance for growth because it depends directly on the individual's structural mass. This
500 parameter contributes biological realism to the state dynamics, but is difficult to measure or
501 estimate directly, especially for fish that spawn multiple times per year, because often little is
502 known about the frequency of spawning. In sensitivity analyses, we found that making this
503 constraint more stringent (e.g., decreasing φ from 0.2 to 0.1) led to increased body sizes at both
504 high and low productivity values (Supp. Fig. 7). Finally, we used estimates of parameters for the
505 metabolic cost function that were measured experimentally for tuna species because of our
506 interest in explaining diversity in tuna growth patterns (Clarke and Johnston 1999). However, to
507 understand if the relatively small effect of increased temperatures on body size in Figure 5 is
508 robust to differences in physiological costs, we conducted sensitivity analyses in which the shape
509 and allometric scaling of costs varied (Supp. Figs. 8 and 9). We confirmed that our choice of
510 parameters for this function had relatively minor influences on growth and reproduction (Supp.
511 Fig. 9).

Our model recovered the three ecological lifestyles of tunas, specifically, the growth, body size, and reproductive patterns that emerged in three environmental scenarios corresponding to each of the three tuna lifestyles outlined in Fig. 3 (Figure 6, Table 2). With the environmental scenario representing the tropical shallow-diving lifestyle, we predicted individual body sizes of less than 100 cm and a longevity of 10 years of age and continuous reproduction at relatively low levels (left column, Figure 6). These predicted traits are similar to those of frigate tuna *Auxis thazard,* a tropical shallow-diving tuna species with small body size. With the environmental scenario matching the tropical deep-diving lifestyle, we predicted growth to sizes well over 200 cm, lifespans of less than 15 years, and continuous reproductive output that increases over the individual's life (middle column, Figure 6, Table 2). While we believe this is broadly consistent with the life histories of tropical deep-diving tuna species such as yellowfin tuna *Thunnus albacares*, lifetime reproductive patterns of these batch-spawning species are not well known (Horswill et al. 2019). In the environmental scenario matching the lifestyle of temperate deep-diving tunas, such as Atlantic bluefin tuna, *Thunnus thunnus,* we predicted the maximum body sizes exceeded 350 cm and individuals were predicted to live much longer than 18 years (right column, Figure 6, Table 2). Spawning was constrained to be seasonal in tunas in the third ecological lifestyle (i.e., spawning could only occur in temperatures above 24 °C, which we specified individuals experienced for three months of the year).

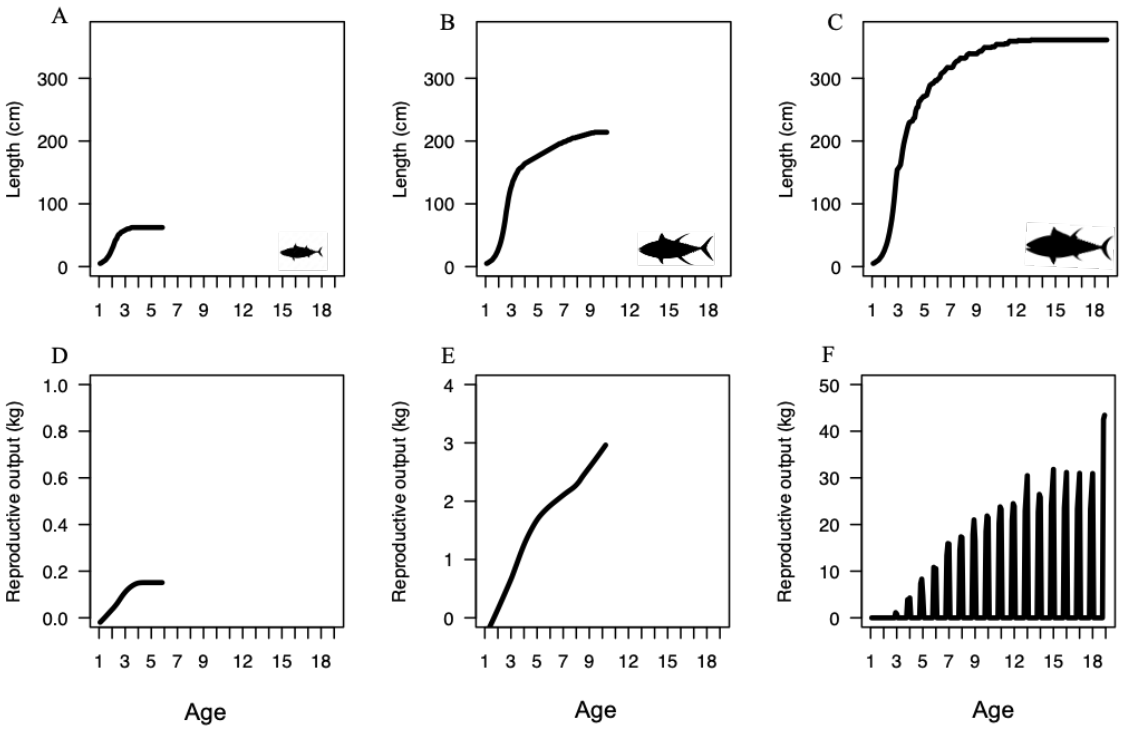

Figure 6. Growth (top row) and reproduction (bottom row) predicted by our model in each of the three representative environmental scenarios corresponding to the three ecological lifestyles of tunas (columns). With the exception of C and F, all curves end at the age when less than 3% of the population is expected to survive, representing the cohort lifespan. A and D represent tropical shallow-diving tuna species such as the frigate tuna *Auxis thazard*. B and E represent tropical deep-diving tuna species such as yellowfin tuna *Thunnus albacares*. C and F represent temperate deep-diving species such as Atlantic bluefin tuna *Thunnus thynnus*, which migrate seasonally from higher latitudes with colder and productive waters to less productive and warmer waters. At age 18, more than 10% of individuals in the temperate deep-diving lifestyle were still alive and are likely to live much longer (C, F). As in Fig. 4, the reproductive output in panels D-E was smoothed using the loess function. Parameters are found in Table 2.

532 *Analysis of seasonality in temperature and spectrum productivity.*

533 The results of the tuna case study yielded an unexpected pattern: when environmental
534 temperature and ecosystem productivity varied seasonally, individuals grew to be 14% larger
535 than the size observed constant scenarios that are otherwise comparable in terms of productivity
536 (κ) and temperature (τ) (Figure 5; Supp. Table 2). To investigate the differential effects of
537 seasonality in temperature (in which species spawn for three months in waters that are 9 degrees
538 warmer than their winter foraging grounds) and in productivity (which increases threefold during
539 winter months), we conducted several follow-up comparisons. In Fig. 7 we plot a range of values
540 for average productivity and the body size and reproduction patterns that emerge in different
541 seasonality scenarios. In Fig. 7A, we compared four scenarios across a range of ecosystem
542 productivities: (i) the scenario when temperature increased during the spawning season but
543 productivity did not change (ii) a threefold increase in productivity for nine months (with
544 constant temperature throughout the year) (iii) three months of seasonality in both temperature
545 and productivity (as in Fig. 6C, F), (ii) predictions from the constant scenario when τ = 16.85 ℃
546 (from Fig. 5). In Fig. 7A, the pattern of increased body size in seasonal environments (relative to
547 constant environments) and consistent increases in length of 12-16% are predicted for a range of
548 seasonality and productivity scenarios (Supp. Table 2). Scenarios with increased temperature or
549 increased productivity alone led to larger body sizes, comparable to the increase expected in the
550 fully seasonal scenario. In Supp. Table 2 we report specific values of body length for different
551 productivity and seasonality combinations to illustrate effects of temperature and productivity
552 alone are consistently comparable to those when combined. In Supp. Fig. 10A, we plot the
553 corresponding expected lifetime reproduction, which is markedly lower in seasonal
554 environments when spawning is limited to three months of the year. From this set of analyses,

we infer that resources and temperature effects on energetic budgets are not the primary drivers of larger body sizes in our model. Rather, the compression of reproductive opportunities into three months of the year, and the temporal separation of reproduction from the most valuable foraging opportunities, favors increased allocation to growth overall.

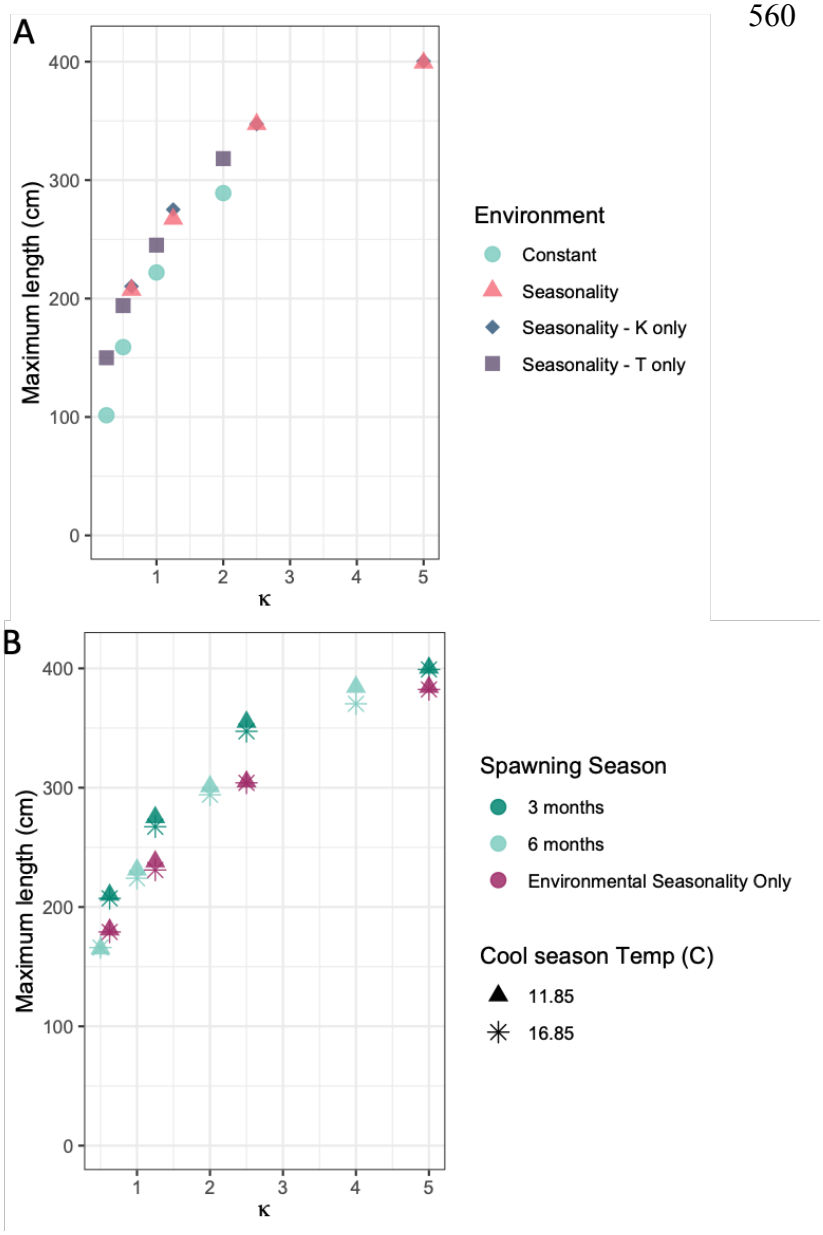

Figure 7. Maximum body length across values of κ and temperature in multiple scenarios varying seasonality in food, temperature, and spawning season duration. In (A) the cool season or baseline temperature was 16.85 °C and spawning activity was limited to three months in the three seasonal scenarios. In (B), the darker teal stars correspond to a three-month spawning season and a winter temperature of 16.85 C, matching the fully seasonal scenario in (A). Magenta points represent individuals that spawn year-round but experience warm, resource poor conditions for three months of the year.

To further understand this effect, in Fig. 7B we compare the maximum lengths expected in six environments that vary in cool season temperature, spawning season length and reproductive constraints. Here, the key contrast is between maximum body sizes when spawning seasons last three months are compared to a spawning season of six months (in which seasonal increases in temperatures and reduction in foraging opportunities lasted twice as long). We also considered a scenario in which spawning occurred year-round, but individuals still experienced seasonal variation in resources and temperature. When individuals spawned in warm, low productivity ecosystems for three months instead of six, asymptotic body lengths were larger, especially at lower values of κ when food is more limited (Fig. 7B). Furthermore, when reproduction was unconstrained, body sizes where again smaller, even though individuals experienced warm, low productivity conditions for three months of the year, most comparable to the constant scenario in Fig. 7A. Cool season temperatures, again, had only minor influences on emergent body sizes. Reproductive output increased with the duration of the spawning season, although it also was strongly affected by productivity and not by temperature (Supp. Fig. 10).

Discussion

We modeled the evolution of growth and reproduction in differing environments, accounting for food web interactions, represented by size spectra, and effects of seasonality in metabolic demands and spawning opportunities. We were able to predict life history variation among the three main ecological lifestyles (ecotypes) of tunas. By unpacking the effects of temporal variation in spawning opportunities, metabolic demands, and foraging opportunities, we predicted that seasonal cycles in resource intake and expenditures can have a greater effect on the evolution of body size than that of temperature on metabolic rate.

585

586 Changes in environmental temperature and ecosystem productivity have been occurring for
587 decades and have been shown to affect fish recruitment, growth, and fishery productivity (Free et
588 al. 2019; Oke et al. 2020). There have been several mechanisms proposed to explain these
589 changes (Fernandes et al. 2020). Early models based on differences in resource intake and
590 metabolic demands predicted that increased temperature will lead to reduced growth and smaller
591 body sizes, i.e., 'shrinking fishes' (Cheung et al. 2008). Yet experimental evidence shows growth
592 is less affected by temperature than reproductive allocation (Wootton et al. 2022), and that
593 metabolic rate can adapt to increased temperatures (Pilakouta et al. 2020). Critically, such
594 physiological models and experimental observations necessarily control for variation in
595 environmental productivity, seasonality, migration, and ecological interactions. To address this
596 gap, we developed a general model incorporating insights from size spectra theory to parametrize
597 the risk of predation (fearscape) and the availability of prey (foodscape) for individuals of
598 different into a model of individual fitness.

599

600 Our model and results build on prior models of life history traits grounded in energy budgets
601 (Ejsmond et al. 2010; Jusup et al 2011) in which increased allocation to reproduction leads to a
602 slowdown in growth rate with age. Alternatively, asymptotic growth patterns have been
603 predicted by physiological models that broadly assume surface uptake areas, relative to the
604 volume of metabolically available mass, leads to intrinsic geometric constraints causing
605 asymptotic growth (von Bertalanffy 1960, Pauly 2010). In our model, multiple (mainly extrinsic)
606 ecological mechanisms led to slowing of growth and emergence of an asymptotic size in each
607 environment. Notably, unlike previous models, in our models the onset of reproduction alone

608 does not correspond immediately to decreasing growth rates and explain where asymptotic body
609 sizes emerge. Instead, the availability of prey, the physical and temporal limits on resource
610 intake, the risk of predation, and constraints on gonad size and reproductive timing all increase
611 the advantage of growing to larger body sizes; these advantages are balanced against metabolic
612 demands and the actual energetic requirements of growth.
613
614 A key difference between our model and other models of life history evolution of fishes in
615 different environmental conditions is that we consider the mass-specific scaling of metabolic
616 costs with temperature in addition to differences in primary production, which drive food-web
617 interactions (White et al. 2022). Across a range of temperatures, our model predicted the benefits
618 of growing large through the foodscape and fearscape outweighed the increase in metabolic costs
619 until very large sizes or very dramatic increases in temperature. For example, although our model
620 predicted smaller body sizes and decreased lifetime reproduction at higher temperatures when
621 both predators and prey were scarce, these differences were relatively small until average
622 temperatures increased by 10-15 ℃. Ecosystem productivity κ had a much stronger influence on
623 our results than any of our other parameters; consistent with expectations, our model predicted
624 larger maximum body sizes, greater reproductive output, and longer lifespans in more productive
625 ecosystems. One exception came when estimating age-specific mortality of each environment,
626 which was more sensitive to our choice of the value representing variation due to predator
627 satiation or efficiency in prey capture (*h,* Eq. 3). However, this process did not substantially
628 change growth trajectories.
629

630 We used variation among tuna ecological lifestyles as a motivation for our model
631 parameterizations and comparisons, while also aiming to provide general insights. We
632 successfully predicted growth patterns that are consistent with species representing each
633 ecological lifestyle of tunas (Fig. 6). Unexpectedly, we found an effect of seasonal variation on
634 body size, where individuals grew larger when they experienced higher productivity or colder
635 temperatures for part of the year (but average productivities were similar). Further investigation
636 revealed this effect is present with seasonal variation in temperature or in productivity alone.
637 These effects were not additive nor interactive (Fig. 7, Supp. Table 2), which rules out
638 explanations based on metabolic costs and strongly supports the conclusion that growth is driven
639 by the limited time available for reproduction, coupled with the opportunity to forage and store
640 energy, but not reproduce, the rest of the year. These results could explain giantism in highly
641 seasonal polar environments. For fishes like tunas, which often exhibit a combination of capital
642 and income breeding, and for which reproduction is determined by temperature, warmer
643 conditions will eventually allow spawning at higher latitudes for longer periods. Our results
644 suggest that cascading effects on their growth are not easily predicted and will depend on how
645 warming waters reverberate through the size spectrum.
646
647 Our model illustrates that predicting responses in growth and reproduction in changing
648 environments is complex, because optimal strategies responding to selective pressures from
649 many factors, including constraints on storage and reproduction, physiology, and the nature of
650 ecosystem fearscapes and foodscapes. For the analyses presented here, we have assumed a static
651 relationship between length and mass, and the conversion of mass to joules (energy density of
652 tissue). Keeping these relationships constant ensured a common currency linking individual

energetic budgets to ecological changes in predation risk and foraging success. Exploring the consequences of these relationships for differences among clades would be a natural follow-up to our study. For example, while we did not directly address the interaction between of fisheries induced selection and growth, it is a rich area of further investigation (Audzijonyte et al. 2016). Plastic or evolutionary responses to fishing potentially include faster growth, earlier maturation rates, and smaller maximum body sizes, but the consequences for marine food webs are complex (Hočevar and & Kuparinen 2021). The framework introduced here potentially could capture how eco-evolutionary feedbacks between fishing mortality, growth and mass relationships, and ecosystem size spectra interactively affect trends in body sizes of focal species. Studies of the interaction between fishing and size spectra have been focused on lake systems where food webs have been studied in greater detail (Perälä and Kuparinen 2020). Understanding how these physiological and ecological processes are linked is necessary to understand how species will respond to different environmental changes and climate change scenarios in the ocean. Our findings suggest that when predicting future growth patterns under projected changes in climate, several ecological and physiological factors, notably primary production prey size and availability and predation risk will play a greater role than temperature in determining trends in body size.

Appendix. Optimization details.

Dynamic programming equations (Eq. 12) are constrained optimization algorithms with the purpose of determining the optimal set of behaviors or decisions that maximize a quantitative metric over time, such as lifetime expected reproductive success. A key property is that the

decisions at one time affect the state variables at the next time. When solving Eq. 12, we consider how the allocation decisions an individual makes during one month of its life affect its future size, energetic reserves (lipid stores) and chances of survival, and find the set of allocation to growth and reproduction that maximizes its fitness in a given environment. We are able to calculate lifetime fitness by solving the equation using backwards iteration. By starting at $t = T - 1$, and assuming there is no possibility of future fitness (i.e., the second term of Eq. 12 is equal to zero for all possible values of length and lipid stores) we can populate the array with the fitness of all possible combinations of length, lipid stores, and allocation strategies at $t = T - 1$; this fitness will be the first term on the right side of Eq. 12. This process is repeated, working backwards, until $t = 1$. We can thereby determine the combination of g and r that maximizes both current fitness at t, and the fitness expected from $t + 1$ until T, given the chance of survival, length, and lipid stores resulting from that particular strategy. Solving Eq. 12 in this way produces an array storing the proportional allocation to growth and reproduction that leads to the highest lifetime fitness, for all possible combinations of size and lipid stores (l and s) for every month until the final time T.

Solving a dynamic programming equation with two state variables, such as Eq. 12, is computationally expensive, and we employed a number of techniques to make the iteration more efficient and to approximate a smooth fitness surface. First, we constrained the parameter space that was evaluated. Specifically, we used an integer index I (with a maximum of I_{max}) to represent lipid stores s, converting the index to values in joules in the dynamic loop. We then related the range of s we explored to each value of l (because lipid stores are constrained by l), by setting

$$s = \frac{0.6 \cdot I^3 \rho a l_{max}{}^3}{I_{max}{}^3}$$

In other words, we adjusted the numerical step size for possible values of *s* to be finer for smaller individuals. Furthermore, we used linear interpolation of state values (Clark and Mangel 2000) when computing expected future fitness in Eq. 12 to minimize discontinuities on the fitness landscape arising from the integer index of energetic state. We did not interpolate length, since its unit (centimeters) was sufficiently fine-grained that there were minimal effects of discontinuities.

We found that sharp transitions in the fitness landscape, such as at threshold values representing constraints, hindered our optimization algorithm. Therefore, we used an asymptotic function for the fitness increment associated with a given level of reproductive output. We let $R(r, s, l, t)$ denote the potential increment in fitness in month *t* when $L(t) = l$, $S(t) = s$, and a fraction of stores *r* is allocated to current reproduction, and assumed that R increased smoothly toward the maximum possible for the given length *l:*

$$R(r, s, l) = \frac{rs}{1 + ({}^{rs}/_{\varphi w(l)})^f} \tag{11}$$

The asymptotic value of this function depends on the value of *f* in the denominator, which controls the abruptness of the constraint on current fitness (Supp. Fig. 2). In other words, the steepness of the multivariate landscape around the fitness optimum is modulated by *f.* For simplicity, we assume $f = 1$ for all results presented hereafter. In that case, when $\varphi w(l) >> \frac{rs}{\rho}$, $R(r, s, l) \sim rs$ and when $rs >> \varphi w(l)$, then $R(r, s, l) \sim \varphi w(l)$.

All programming was done using R 4.1.1 and all code and model outputs will be available. We ran the code to solve the dynamic programming equation and simulate the individual life histories using Rscript commands from the Linux shell of a 2019 MacPro with 16 cores and 96 GB of RAM. Jobs were run in parallel and the runtime of each job was between 60 and 120 minutes. The results of each job are presented in the figures summarizing growth, reproduction, and survival data; these analyses and figures were produced in the Rstudio IDE.

Data Archiving statement: All code and model outputs for this study are available in a github repository and will be archived upon publication.

References

Álvarez-Noriega M., White C.R., Kozłowski J., Day T., Marshall D.J. 2023. Life history optimisation drives latitudinal gradients and responses to global change in marine fishes. PLoS Biol 21(5): e3002114.

Andersen, K. H. 2019. *Fish Ecology, Evolution, and Exploitation: A New Theoretical Synthesis.* Princeton University Press, Princeton.

Andersen, K. H., Jacobsen, N. S., Farnsworth, K. D., and J. Baum. 2016. The theoretical foundations for size spectrum models of fish communities. *Canadian Journal of Fisheries and Aquatic Sciences* 73:575–588.

Audzijonyte, A., Fulton, E., Haddon, M., Helidoniotis, F., Hobday, A.J., Kuparinen, A., Morrongiello, J., Smith, A.D., Upston, J. and Waples, R.S., 2016. Trends and management implications of human-influenced life-history changes in marine ectotherms. *Fish and Fisheries*, *17*(4), pp.1005-1028.

Audzijonyte, A., Richards, S.A., Stuart-Smith, R.D., Pecl, G., Edgar, G.J., Barrett, N.S., Payne, N. and Blanchard, J.L., 2020. Fish body sizes change with temperature but not all species shrink with warming. *Nature Ecology & Evolution*. 4:809-814.

Audzijonyte, A. and Richards, S.A., 2018. The energetic cost of reproduction and its effect on optimal life-history strategies. *American Naturalist*. 192:E150-E162.

Audzijonyte, A., Jakubavičiūtė, E., Lindmark, M., and Richards S.A. 2022. Mechanistic Temperature-Size Rule Explanation Should Reconcile Physiological and Mortality Responses to Temperature. *The Biological Bulletin* 2022 243:2, 220-238

Barnes, W., Maxwell, D., Reuman, D.C., and Jennings, S., 2010. Global patterns in predator-prey size relationships reveal size dependency of trophic transfer efficiency. *Ecology* 91:222-232.

Benoît, E., and M. J. Rochet. 2004. A continuous model of biomass size spectra governed by predation and the effects of fishing on them. *Journal of Theoretical Biology* 226:9-21.

Bernal, D. 2011. Physiological specializations of different fish groups. Pelagic fishes. Pages 1887-1902 *in* Farrell AP (ed) *Encyclopedia of Fish Physiology: From Genome to Environment,* Vol 3. Academic Press, San Diego.

Bernal, D., Sepulveda C., Musyl, M., Brill, R. (2009) The eco- physiology of swimming and movement patterns of tunas, billfishes, and large pelagic sharks. Pages 436–483 *in* Domenici P, Kapoor BG (eds) *Fish Locomotion: an Etho-Ecological Approach*. Science Publishers, Enfield.

Bernal, D., Brill, R.W., Dickson, K.A. and H.A. Shiels. 2017. Sharing the water column: physiological mechanisms underlying species-specific habitat use in tunas. *Reviews in Fish Biology and Fisheries* 27:843-880.

Bernhardt, J.R., Sunday, J.M. and M.I. O'Connor. 2018. Metabolic theory and the temperature-size rule explain the temperature dependence of population carrying capacity. *American Naturalist.* 192:687-697.

Beverton, R. J. H., and S. J. Holt. 1959. A review of the lifespans and mortality rates of fish in nature, and their relation to growth and other physiological characteristics. Pages 142–177 *in* CIBA Foundation Colloquium on Ageing.

Bigman, J.S., M'Gonigle, L., Wegner, N.C. and Dulvy, N.K. 2021. Respiratory capacity is twice as important as temperature in driving patterns of metabolic rate across the vertebrate tree of life. *Science Advances* 7: eabe5163.

Blanchard, J. L., Heneghan, R. F., Everett, J. D. , Trebilco, R. and A. J. Richardson. 2017. From bacteria to whales: using functional size spectra to model marine ecosystems. *Trends in Ecology & Evolution.* 32:174-186.

Blanchard, J. L., Jennings, S., Law, R., Castle, M.D., McCloghrie, P., Rochet, M.J., and E. Benoît. 2009. How does abundance scale with body size in coupled size-structured food webs? *Journal of Animal Ecology*. 78:270-280.

Blanchard, J.L., Jennings, S., Holmes, R., Harle, J., Merino, G., Allen, J.I., Holt, J., Dulvy, N.K. and M. Barange. 2012. Potential consequences of climate change for primary production and fish production in large marine ecosystems. *Phil. Trans. Roy. Soc. B* 367:2979-2989.

Brown, J. H., J. F. Gillooly, A. P. Allen, V. M. Savage, and G. B. West. 2004. Toward a metabolic theory of ecology. *Ecology.* 85:1771-1789.

Chapman, E. W., Kørgensen, C., and M. E. Lutcavage. 2011. Atlantic bluefin tuna (*Thunnus thynnus*): a state-dependent energy allocation model for growth, maturation, and reproductive investment. *Canadian Journal of Fisheries and Aquatic Sciences* 68:1934–1951.

Charnov, E. L., Berrigan, D., and R. J. H. Beverton. 1991. Dimensionless numbers and the assembly rules for life histories. *Phil. Trans. Roy. Soc. B* 332:41-48.

Charnov, E. L., and J. R. Krebs. 1974. On clutch-size and fitness. *Ibis.* 116:217-219.

Cheung, W.W., Close, C., Lam, V., Watson, R., and D. Pauly 2008. Application of macroecological theory to predict effects of climate change on global fisheries potential. *Marine Ecology Progress Series*. 365:187-197.

Christensen, A. and Andersen, K.H., 2011. General classification of maturation reaction-norm shape from size-based processes. Bulletin of Mathematical Biology, 73(5): 1004-1027.

Cichoń, M. and Kozłowski, J., 2000. Ageing and typical survivorship curves result from optimal resource allocation. Evolutionary Ecology Research, 2(7): 857-870.

Clark, C. W., and M. Mangel. 2000. Dynamic state variable models in ecology: methods and applications. Oxford University Press, Oxford.

Clarke, A. 2006. Temperature and the metabolic theory of ecology. *Functional Ecology* 20:405-412.

Clarke, A., and N. M. Johnston. 1999. Scaling of metabolic rate with body mass and temperature in teleost fish. *Journal of Animal Ecology*. 68: 893-905.

Conover, D. O., and S. B. Munch. 2002. Sustaining fisheries yields over evolutionary timescales. *Science* 297:94–96.

Daufresne, M, Lengfellner, K., and U. Sommer. 2009. Global warming benefits the small in aquatic ecosystems. *Proc. Nat. Acad. Sci.* 106:12788–12793.

Dickson, K.A., and Graham, J.B. 2004. Evolution and consequences of endothermy in fishes *Physiological and Biochemical Zoology* 77: 998-1018.

Ejsmond, M.J., Czarnołęski, M., Kapustka, F. and Kozłowski, J., 2010. How to time growth and reproduction during the vegetative season: an evolutionary choice for indeterminate growers in seasonal environments. *The American Naturalist* 175(5): 551-563.

Fernandes, J.A., Rutterford, L., Simpson, S.D., Butenschön, M., Frölicher, T.L., Yool, A., Cheung, W.W. and Grant, A., 2020. Can we project changes in fish abundance and distribution in response to climate? *Global Change Biology.* 26:3891-3905.

Free, C.M., Thorson, J.T., Pinsky, M.L., Oken, K.L., Wiedenmann, J. and Jensen, O.P. 2019. Impacts of historical warming on marine fisheries production. *Science.* 363: 979-983.

Froese R. 2006. Cube law, condition factor and weight-length relationships: history, meta-analysis and recommendations. *Journal of Applied Ichthyology* 22: 241-253

Gadgil, M., and W. H. Bossert. 1970. Life historical consequences of natural selection. *American Naturalist* 104:1-24.

Giacomini, H.C., Shuter, B.J. and Lester, N.P., 2013. Predator bioenergetics and the prey size spectrum: Do foraging costs determine fish production? *Journal of Theoretical Biology* 332: 249-260.

Gillooly, J. F., Brown, J. H., West, G. B., Savage, V. M., and E. L. Charnov. 2001. Effects of size and temperature on metabolic rate. *Science.* 293:2248–2251.

Gislason, H., Daan, N. Rice, J. C., and J. G. Pope. 2010. Size, growth, temperature and the natural mortality of marine fish. *Fish and Fisheries* 11:149–158.

Hilborn, R. and Mangel, M. 1997. *The Ecological Detective.* Princeton University Press, Princeton, NJ.

Hočevar, S., & Kuparinen, A. (2021). Marine food web perspective to fisheries-induced evolution. *Evolutionary Applications*, 14, 2378– 2391.

Horswill, C., H. K. Kindsvater, M. J. Juan-Jordá, N. K. Dulvy, M. Mangel, and J. Matthiopoulos. 2019. Global reconstruction of life-history strategies: A case study using tunas. *Journal of Applied Ecology* 56:855-865.

Houston, A., C. Clark, J. McNamara, and M. Mangel. 1988. Dynamic Models in Behavioural and Evolutionary Ecology. *Nature.* 332:29-34

Houston, A., and J. McNamara. 1999. *Models of Adaptive Behaviour*. Cambridge University Press.

Hulthén, K., Hill, J.S., Jenkins, M.R. and Langerhans, R.B., 2021. Predation and resource availability interact to drive life-history evolution in an adaptive radiation of livebearing fish. *Frontiers in Ecology and Evolution*, 9, p.619277.

Jørgensen, C., K. Enberg, and M. Mangel. 2016. Modelling and interpreting fish bioenergetics: a role for behaviour, life-history traits and survival trade-offs. *Journal of Fish Biology* 88:389–402.

Jørgensen, C., and Ø. Fiksen. 2006. State-dependent energy allocation in cod (*Gadus morhua*). *Canadian Journal of Fisheries and Aquatic Sciences* 63:186–199.

Juan-Jordá, M. J., I. Mosqueira, J. Freire, and N. K. Dulvy. 2013. The Conservation and Management of Tunas and Their Relatives: Setting Life History Research Priorities. *PLoS ONE* 8:e70405.

Juan-Jordá, M.J., Mosqueira, I., Freire, J., Ferrer-Jordá, E. and Dulvy, N.K. 2016. Global scombrid life history data set. *Ecology*, 97: 809-809.

Jusup, M., Klanjscek, T., Matsuda, H., Kooijman, S.A.L.M. 2011. A Full Lifecycle Bioenergetic Model for Bluefin Tuna. *PLoS ONE* 6(7): e21903.

Kindsvater, H.K., Alonzo, S.H., Mangel, M. and Bonsall, M.B., 2010. Effects of age-and state-dependent allocation on offspring size and number. *Evolutionary Ecology Research*, 12(3), pp.327-346.

Kingsolver, J. G., and R. B. Huey. 2008. Size, temperature , and fitness: three rules. *Evolutionary Ecology Research* 10:251–268.

Kiørboe, T., and A. G. Hirst. 2014. Shifts in mass scaling of respiration, feeding, and growth rates across life-form transitions in marine pelagic organisms. *American Naturalist* 183:E118-E130.

Kitchell, J.F., Neill, W.H., Dizon, A.E., and J.J. Magnuson. 1978. Bioenergetic Spectra of Skipjack and Yellofin Tunas. In:Sharp, G.D., Dizon, A.A. (Eds.), *The Physiological Ecology of Tunas.* Academic Press.

Kozłowski, J., 1992. Optimal allocation of resources to growth and reproduction: implications for age and size at maturity. *Trends in Ecology and Evolution*, 7(1):15-19.

Kozlowski, J. 1996. Optimal allocation of resources explains interspecific life-history patterns in animals with indeterminate growth *Proc. R. Soc. B.* 263: 559-566.

Kozłowski, J. and Teriokhin, A.T., 1999. Allocation of energy between growth and reproduction: the Pontryagin Maximum Principle solution for the case of age-and season-dependent mortality. *Evolutionary Ecology Research* 1(4): 423-441

Law, R., M. J. Plank, A. James, and J. L. Blanchard. 2009. Size-spectra dynamics from stochastic predation and growth of individuals. *Ecology* 90:802-811.

Lika, K. and Kooijman, S.A., 2003. Life history implications of allocation to growth versus reproduction in dynamic energy budgets. Bulletin of Mathematical Biology, 65(5), pp.809-834.

Oke, K.B., Cunningham, C.J., Westley, P.A.H., Baskett, M.L., Carlson, S.M., Clark, J., Hendry, A.P., Karatayev, V.A., Kendall, N.W., Kibele, J. ,Kindsvater, H.K., Kobayashi, K.M., Lewis, B., Munch, S., Reynolds, J.D., Vick, G.D., and E.P. Palkovacs. 2020. Recent declines in salmon body size impact ecosystems and fisheries. *Nature communications*, 11:1-13.

Perälä, T, Kuparinen, A. Eco-evolutionary dynamics driven by fishing: From single species models to dynamic evolution within complex food webs. *Evol Appl*. 2020; 13: 2507– 2520.

Perrin, N. and Sibly, R.M., 1993. Dynamic models of energy allocation and investment. Annual Review of Ecology and Systematics, 24: 379-410.

Perrin, N., Sibly, R.M. and Nichols, N.K., 1993. Optimal growth strategies when mortality and production rates are size-dependent. Evolutionary Ecology, 7(6), pp.576-592.

Mangel, M. 2006. The Theoretical Biologist's Toolbox : Quantitative Methods for Ecology and Evolutionary Biology. Cambridge University Press.

Mangel, M. 2015. Stochastic dynamic programming illuminates the link between environment, physiology, and evolution. *Bulletin of Mathematical Biology* 77:857-877.

Mangel, M. and C. W. Clark. 1988. *Dynamic Modelling in Behavioral Ecology.* Princeton University Press, Princeton.

Monsch, K.A. 2000 *The Phylogeny of the Scombroid Fishes.* PhD thesis, University of Bristol p 272.

Neubauer, P., and K. H. Andersen. 2019. Thermal performance of fish is explained by an interplay between physiology, behaviour and ecology. *Conservation Physiology* 7:coz025

Pauly D. 2010. Gasping fish and panting squids: oxygen, temperature and the growth of water-breathing animals. International Ecology Institute, Germany.

Pilakouta, N, Killen, SS, Kristjánsson, BK, et al. 2020. Multigenerational exposure to elevated temperatures leads to a reduction in standard metabolic rate in the wild. *Funct Ecol*. 34:1205-1214.

Pignalosa, P., Pappalardo, L., Gioacchini, G., Carnevali, O. 2020. Length-weight relationships and a new length conversion factor for Atlantic Bluefin tuna (*Thunnus thynnus L.*) caught in the Mediterranean Sea. *Collect. Vol. Sci. Pap. ICCAT,* 76(2): 138-146.

Quince, C., Abrams, P.A., Shuter, B.J. and Lester, N.P., 2008. Biphasic growth in fish I: theoretical foundations. *Journal of Theoretical Biology*, 254(2): 197-206.

Schaefer, K.M. 2001. Reproductive biology of tunas. *Fish Physiology.* 19: 225-270.

Schaefer K.M., Fuller D.W., and B.A. Block 2009. Vertical movements and habitat utilization of skipjack (*Katsuwonus pelamis*), yellowfin (*Thunnus albacares*), and bigeye (*Thunnus obesus*) tunas in the Equatorial Eastern Pacific Ocean, ascertained through archival tag data. Pages 121-144 *in* Nielsen, J.L., Arrizabalaga, H., Fragoso, N., Hobday, A., Lutcavage, M., Sibert, J. (Eds.), *Tagging and Tracking of Marine Animals with Electronic Devices*. Springer, New York.

Sheldon, R.W., Prakash, A. and Sutcliffe Jr., W.H. 1972. The distribution of particles in the ocean. *Limnology and Oceanography.* 17:327-340.

Sheldon, R.W., Sutcliffe Jr., W.H., and M.A. Paranjape. 1977. Structure of pelagic food chain and relationship between plankton and fish production. *Journal of the Fisheries Research Board of Canada*. 34: 2344-2353.

Shuter, B.J., Giacomini, H.C., de Kerckhove, D. and Vascotto, K., 2016. Fish life history dynamics: shifts in prey size structure evoke shifts in predator maturation traits. *Canadian Journal of Fisheries and Aquatic Sciences*. 73(4): 693-708.

Southwood, T.R.E. 1977. Habitat, the Templet for Ecological Strategies? *Journal of Animal Ecology*. 46:337-365.

Sprules, W. G., and L. E. Barth. 2016. Surfing the biomass size spectrum: some remarks on history, theory, and application. *Canadian Journal of Fisheries and Aquatic Sciences* 73:477-495.

Thygesen, U.H., Farnsworth, K.D., Andersen, K.H., Beyer, J.E. 2005. How optimal life history changes with the community size-spectrum. *Proc. R. Soc. B*. 272:1323-1331.

Trebilco, R., Baum, J. K., Salomon, A. K., and N. K. Dulvy. 2013. Ecosystem ecology: Size-based constraints on the pyramids of life. *Trends in Ecology & Evolution*. 28:423-431.

Ursin, E. 1973. On the prey size preferences of cod and dab. *Meddelelser fra Danmarks Fiskeri- og Havundersøgelser* 7: 85–98.

Varpe, Ø., 2017. Life history adaptations to seasonality. *Integrative and comparative biology*, *57*(5), pp.943-960.

von Bertalanffy L. 1960. Principles and theory of growth. Pages 137-259 *in* Nowinski, W.W., Ed., *Fundamental Aspects of Normal and Malignant Growth*, Elsevier, Amsterdam.

Walsh, M. R., and D. N. Reznick. 2009. Phenotypic diversification across an environmental gradient: a role for predators and resource availability on the evolution of life histories. *Evolution* 63:3201–3213.

White, C.R., Alton, L.A., Bywater, C.L., Lombardi, E.J. and Marshall, D.J., 2022. Metabolic scaling is the product of life-history optimization. *Science*, *377*(6608), pp.834-839.

Wong, S., Bigman, J.S., and N.K. Dulvy. 2021. The metabolic pace of life histories across fishes. *Proc. R. Soc. B*. 288:20210910.

Wootton, H.F., Morrongiello, J.R., Schmitt, T. & Audzijonyte, A. 2022. Smaller adult fish size in warmer water is not explained by elevated metabolism. Ecology Letters, 25, 1177– 1188.

Yanco, S.W., Pierce, A.K. and Wunder, M.B. 2022. Life history diversity in terrestrial animals is associated with metabolic response to seasonally fluctuating resources. Ecography. 2022:e05900

1043 **Table 1**. Description of parameters and variables

Parameter or Variable	Description	Value
w	Body mass in kg	-
N	Number of individuals in a size category (or trophic level) when considering a Sheldon size spectrum	-
B	Absolute biomass in a size category (or trophic level) when considering a Sheldon size spectrum	-
κ	The spectrum parameter, which defines the total biomass of organisms of the smallest body size w in a given ecosystem; Andersen (2019) gives an estimate of 10 gained by averaging over all Predator-Prey Mass Ratio estimates measured from gut contents. We vary it to represent ecosystem differences in overall ecosystem productivity	Varies
$Bprey$	Biomass of prey expected by a focal individual	-
μ_p	Instantaneous risk of mortality due to predation, which depends on body mass and position in the size spectrum	-
h	Predation risk, comprised of predator satiation estimates (estimated from gut contents) and predator preference (or effectiveness) for consuming prey of a given mass (Andersen 2019)	4, 8
τ	Temperature of the environment (in degrees Kelvin except where noted)	285-300
C	Metabolic requirements (costs) that scale with mass and temperature	-
c	Normalization constant scaling metabolic costs (in J), based on metabolic rate data from tunas (Kitchell et al. 1978)	5×10^{16}
k_B	Boltzmann constant, relating particle energy to temperature in units of m^2 kg s^{-2} K^{-1}	1.3×10^{-23}
E	The average activation energy for the rate limiting enzymes in metabolism in units of joules; from the metabolic theory of ecology (Gillooly et al. 2001).	1.04×10^{-19}
θ	Metabolic scaling exponent; values vary among clade, here we use a value reported for tunas (Clarke and Johnston 1999)	0.66
ρ	The energy density of tuna body mass in our model in J/kg (estimated empirically and reported in Chapman et al. 2011)	4.2×10^{6}
t	Time in monthly time steps in the dynamic model	-
T_{max}	Maximum lifespan in months	216
l, $L(t)$	Body length (in cm) This is a dynamic state variable but can only increase with time. The maximum value possible is 400 cm. For a specific value, we use the capital letter notation.	-
s, $S(t)$	Lipid stores (in joules) – this is a dynamic state variable representing energy stores that can be used for metabolism, growth, and reproduction.	-
a	Scale coefficient relating length to structural mass, similar to values estimated empirically for bluefin tuna and reported in Pignalosa et al. (2020).	1.0×10^{-5}
$w(t)$	Structural mass of the individual (in kg) at time t – this depends on $L(t)$	-
υ	The fraction of structural mass that determines the critical threshold of energetic mass needed for survival	0.1
φ	The fraction of structural mass that determines the maximum possible reproductive output in a monthly time step	0.2
γ_{pred}	Survival from predation from one month to the next	
γ_s	Survival, given that the individual has sufficient energy reserves to meet metabolic requirements and avoid starvation	
g	Proportion of lipid stores allocated to growth (this allocation decision is optimized by the dynamic programming equation); can take values between 0 and 1	
r	Proportion of lipid stores allocated to reproduction (this allocation decision is optimized by the dynamic programming equation); can take values between 0 and 1 and the sum of g and r cannot exceed one.	
$R(l,s,t)$	Current fitness, the product of lipid stores and the optimal allocation to reproduction, r	
$V(l,s,t)$	Expected accumulated lifetime reproduction from time t onwards, given that $L(t) = l$ and $S(t) = s$	

1044
1045
1046
1047

Table 2

Parameter values for environmental scenarios corresponding to the three ecological lifestyles of tunas described in Fig. 3, with corresponding predicted body size and maximum observed fork length (cm) for three representative species (data from Juan-Jordá et al. 2016).

Lifestyle	**Environment**	**Baseline or winter temp**	**Yearly mean κ**	***h***	**Predicted body size**	**Representative species**	**Reported range of body sizes**
Tropical shallow	Constant	26.85 C	0.1	8	62 cm	Frigate tuna	40-60 cm
Tropical deep diving	Constant	21.85 C	1	8	214 cm	Yellowfin tuna	125-231 cm
Temperate deep diving	Seasonal	11.85	2.5	12	361 cm	Bluefin tuna	203-427 cm

Supplemental Table 1. Model outputs corresponding to points in main text Figure 6. All scenarios had constant environments.

Temperature τ in ℃	κ	Lifetime reproductive output (kg)	Maximum body length (cm)
11.85	0.25	2.15	109.5
11.85	0.5	5.87	173
11.85	1	15.51	224
11.85	2	38.94	289.1
11.85	5	123.77	390.4
16.85	0.25	2.08	101.5
16.85	0.5	5.9	159
16.85	1	15.2	222
16.85	2	37.97	289
16.85	5	121.95	384.3
21.85	0.25	2.02	98.4
21.85	0.5	5.65	159
21.85	1	14.73	214
21.85	2	36.93	282
21.85	5	119.28	380.3
26.85	0.25	1.85	92.4
26.85	0.5	5.33	151
26.85	1	13.85	202
26.85	2	35.15	274
26.85	5	115.73	373.4

Supplemental Table 2. Precise values for body lengths predicted in varying seasonality scenarios for the same value of average κ. These data are complementary to Figure 7, where scenarios that are constant or have seasonality in τ have a different average productivity κ. The differences between different seasonal scenarios at lower average productivity (κ = 1.25) disappear at higher average productivity (κ = 2.5). This suggests that the multiple factors leading to the optimization of the growth-reproduction tradeoffs make the fitness landscape more complex when productivity is lower.

Environment	κ	Length (cm)
Constant	1.25	238.1
Seasonality - κ only	1.25	275.2
Seasonality - τ only	1.25	272.2
Seasonality	1.25	267.3
Constant	2.5	305.1
Seasonality - κ only	2.5	347.4
Seasonality - τ only	2.5	347.4
Seasonality	2.5	347.2

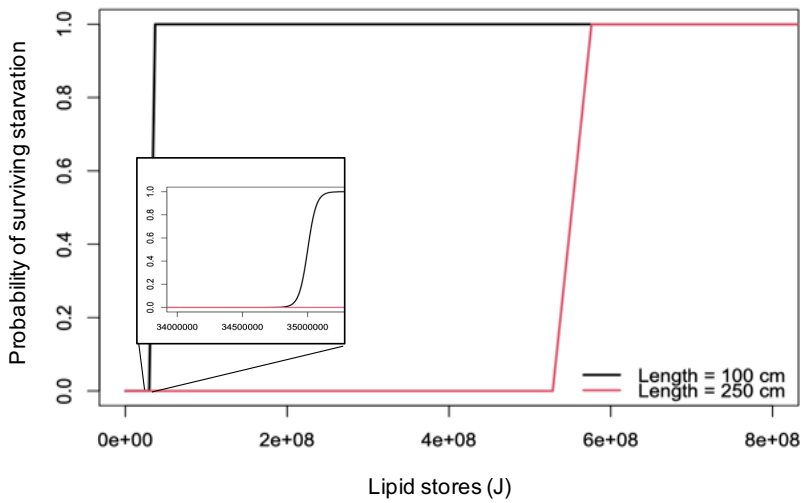

Supplementary Figure 1. Main panel: The sigmoid relationship between lipid stores (in joules) and survival for individuals of different lengths. The threshold amount of energy required for metabolic maintenance is a fixed proportion of body mass. The probability of avoiding starvation $\gamma_s(s, l)$ is a logistic function of mass given in Eq. 11. Inset: closeup of the x-axis in the region encompassing the smaller threshold.

1089
1090

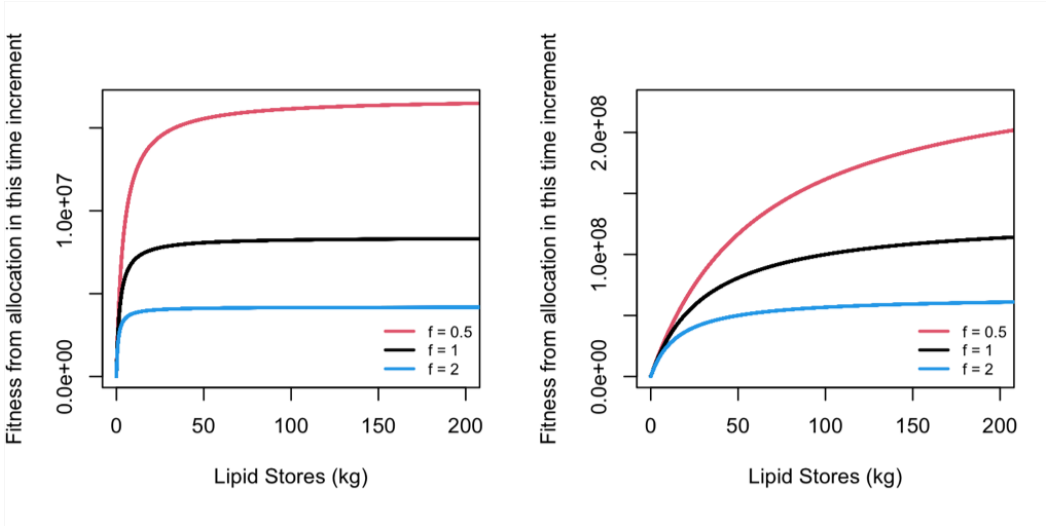

Supplementary Figure 2. The fitness increment expected with different amounts of lipid reserves (energy stores) Left panel: Fitness increment for an individual of 100 cm. Right panel: Fitness increment for an individual of 250 cm. We show the shape of the function for three values of *f* but for all analyses here we used *f* = 1.

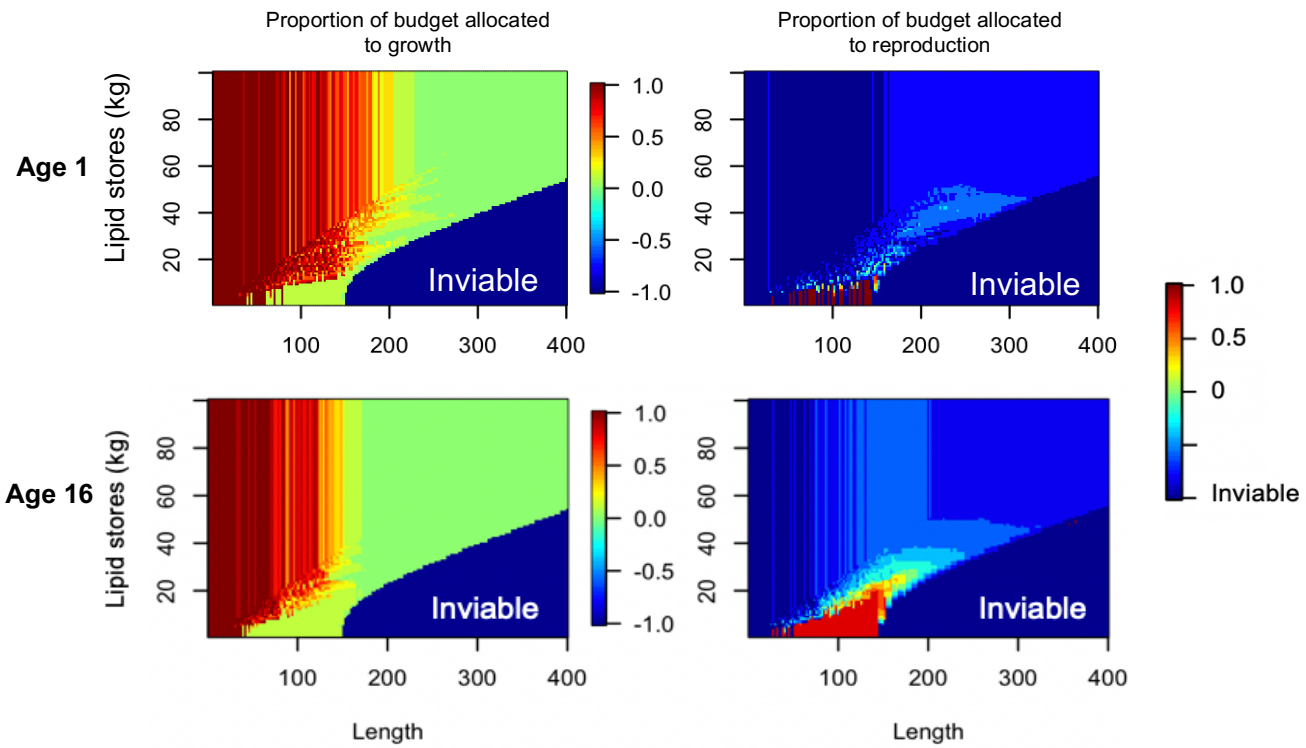

Supplementary Figure 3. Example rules for allocation to growth and reproduction for ages 1 and 16. The inviable region (dark blue) represents parameter space where remaining stores are insufficient for survival, given the individual's length (in other words, energetic requirements for maintenance are not met). Comparing panels within rows shows differences between allocation to growth and reproduction as a function of state and length. Comparing panels within columns shows how the tradeoff between growth and reproduction changes with age. Note that the striations come from the discretization of allocation values of g and r in Eq. 12.

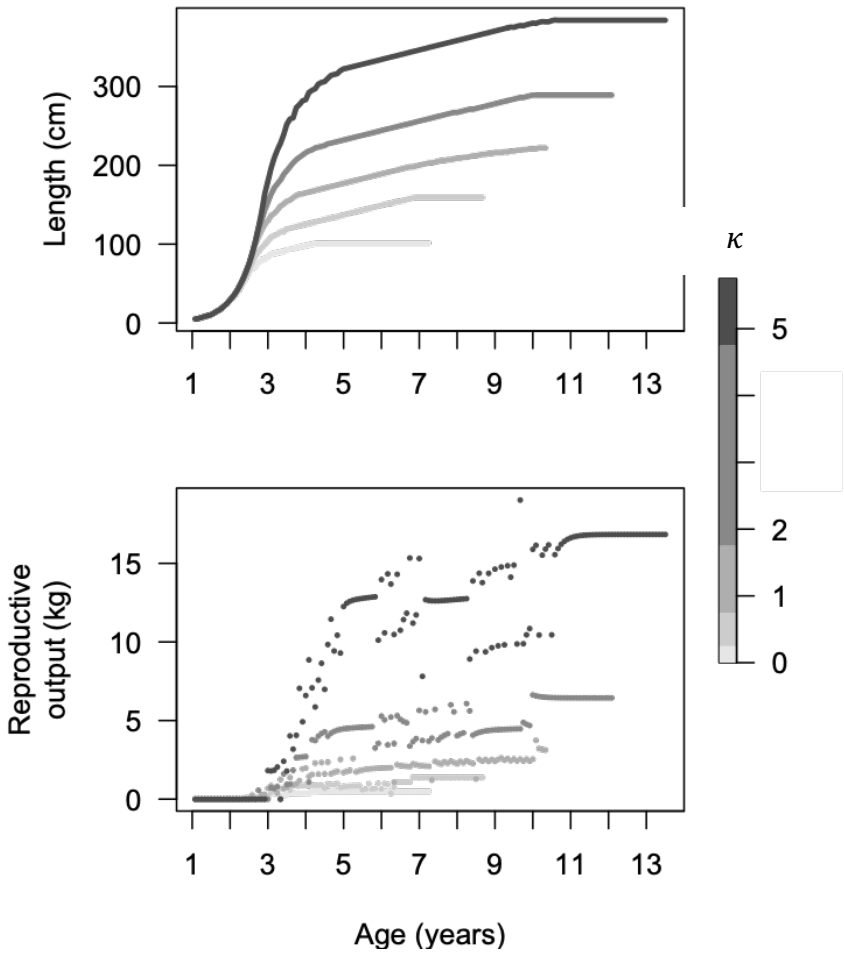

Supplementary Figure 4. Top: The emergent pattern of survival to age at different levels of κ. Bottom: The natural log of survival to age. Dashed horizonal line shows the cutoff past which less than 3% of individuals will survive. For all results here, $h = 8$ and $\tau = 16.85$℃

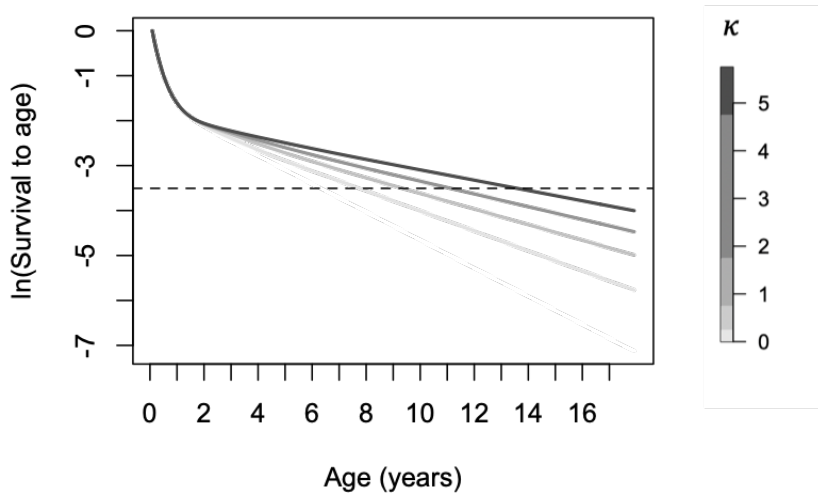

Supplementary Figure 5. The emergent pattern of ln(survival) to age at different levels of κ. Dashed horizonal line shows the cutoff past which less than 3% of individuals will survive. For all results here, h = 8 and $\tau = 16.85$°C.

1101
1102
1103

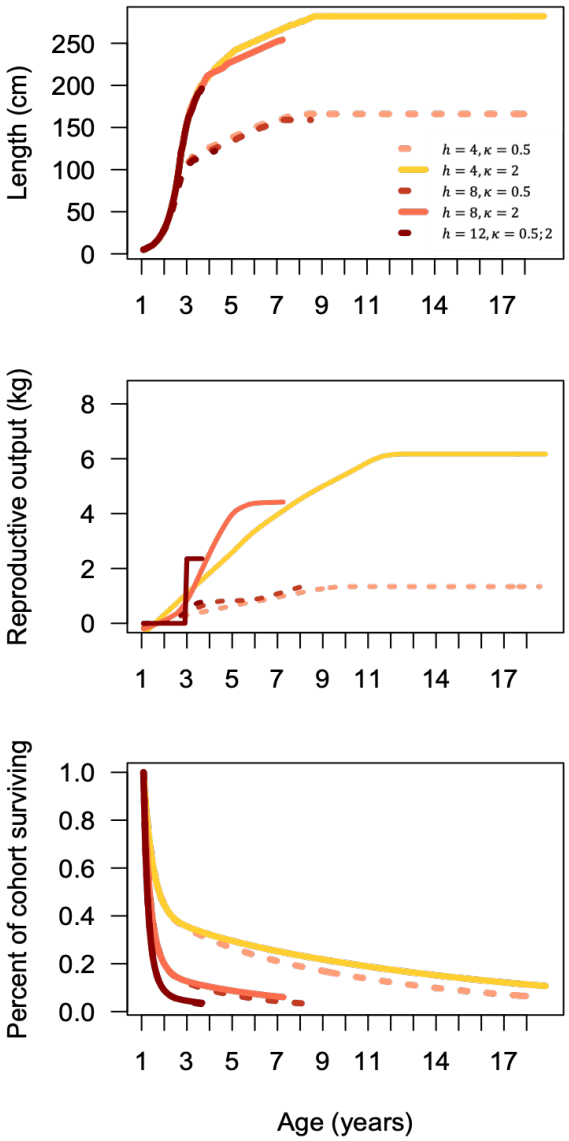

Supplementary Figure 6. The emergent patterns of growth, reproduction, and survival that emerge when h varies. We contrast two values of κ to highlight that it is still the main driver of variation in body size, although h affects lifespan. In all scenarios, $\tau = 16.85°C$. Note that for results presented elsewhere, $h = 8$ except where noted.

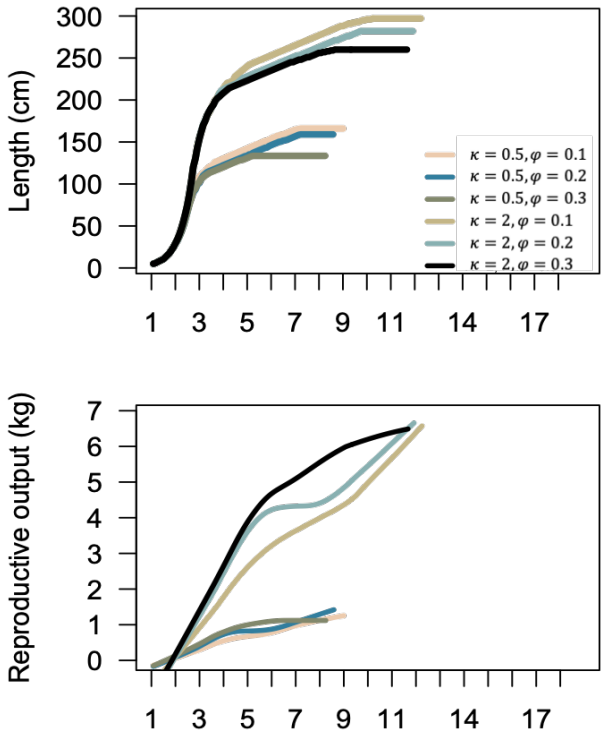

Supplementary Figure 7. Growth curves showing the effect of changes in the reproductive capacity φ, for two values of κ. As the reproductive constraint increases (the fraction of the body cavity that can be devoted to gonad decreases from 0.2 to 0.1), selection favors the evolution of larger body sizes. In all scenarios, $\tau = 16.85$℃. Note that for all results presented elsewhere, $\varphi = 0.2$.

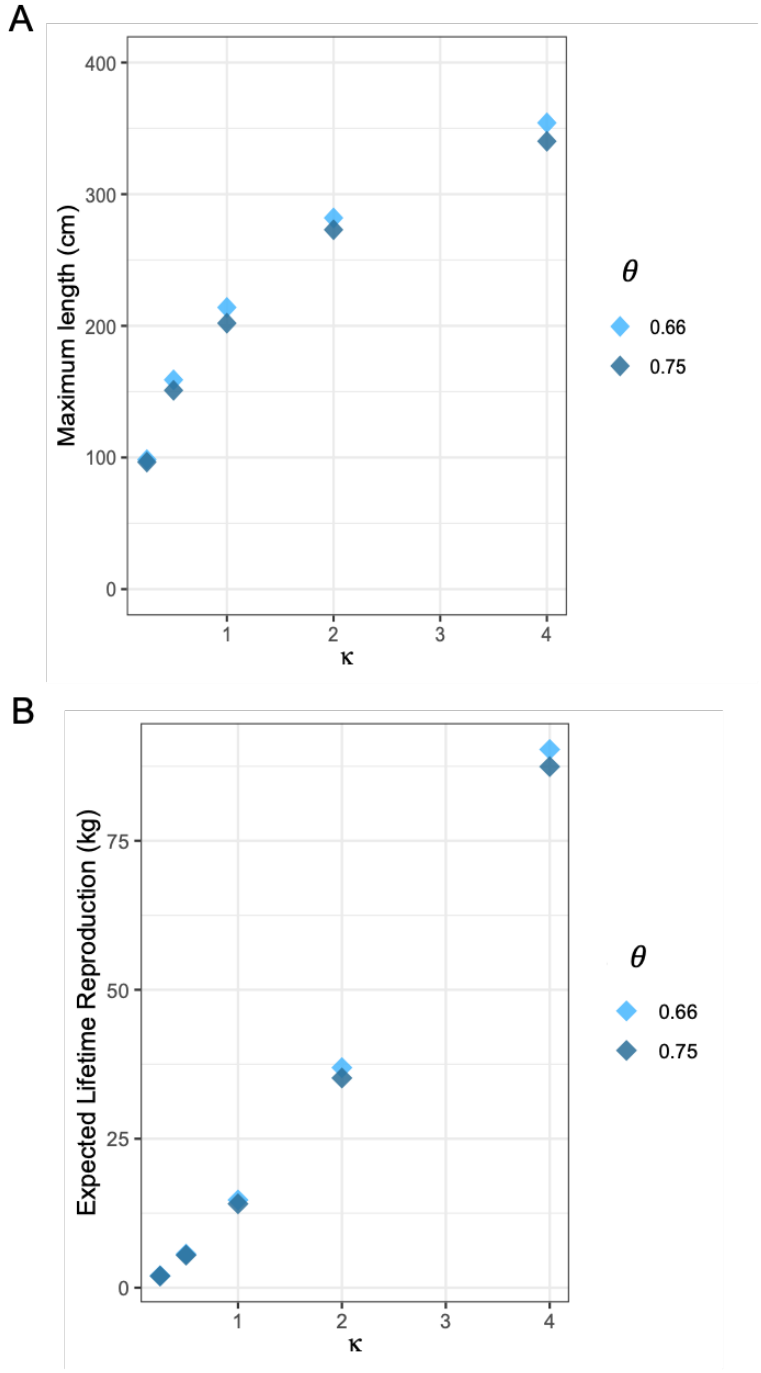

Supplementary Figure 8. Body size and lifetime reproduction for several values of κ and θ (the allometric exponent in the metabolic cost function). For all scenarios, temperature is constant year-round at 21.85°C.

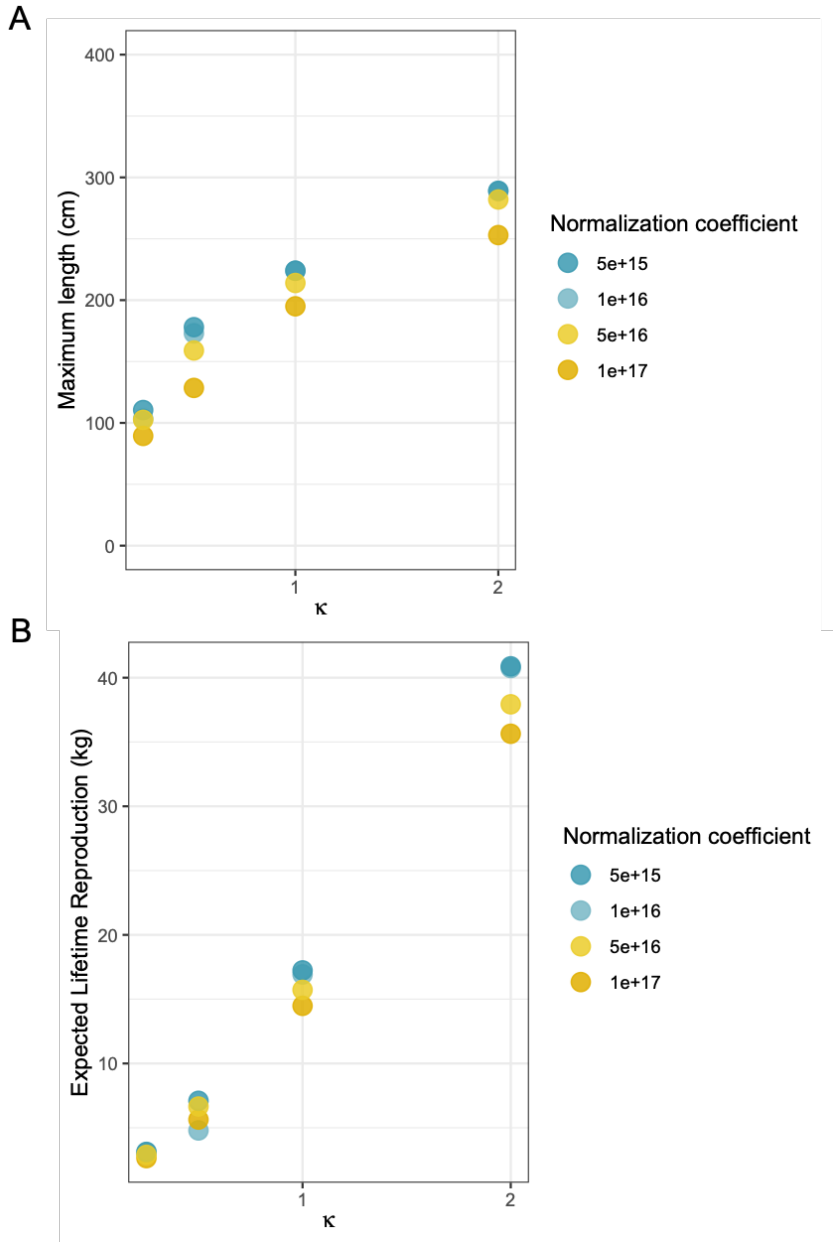

Supplementary Figure 9. Body size and lifetime reproduction for several values of κ and c (the normalization constant in the metabolic cost function). The estimate of c used elsewhere (5×10^{16}) comes from metabolic rate data from tunas (Clarke and Johnston 1999). For all scenarios, temperature is constant year-round at 21.85°C.

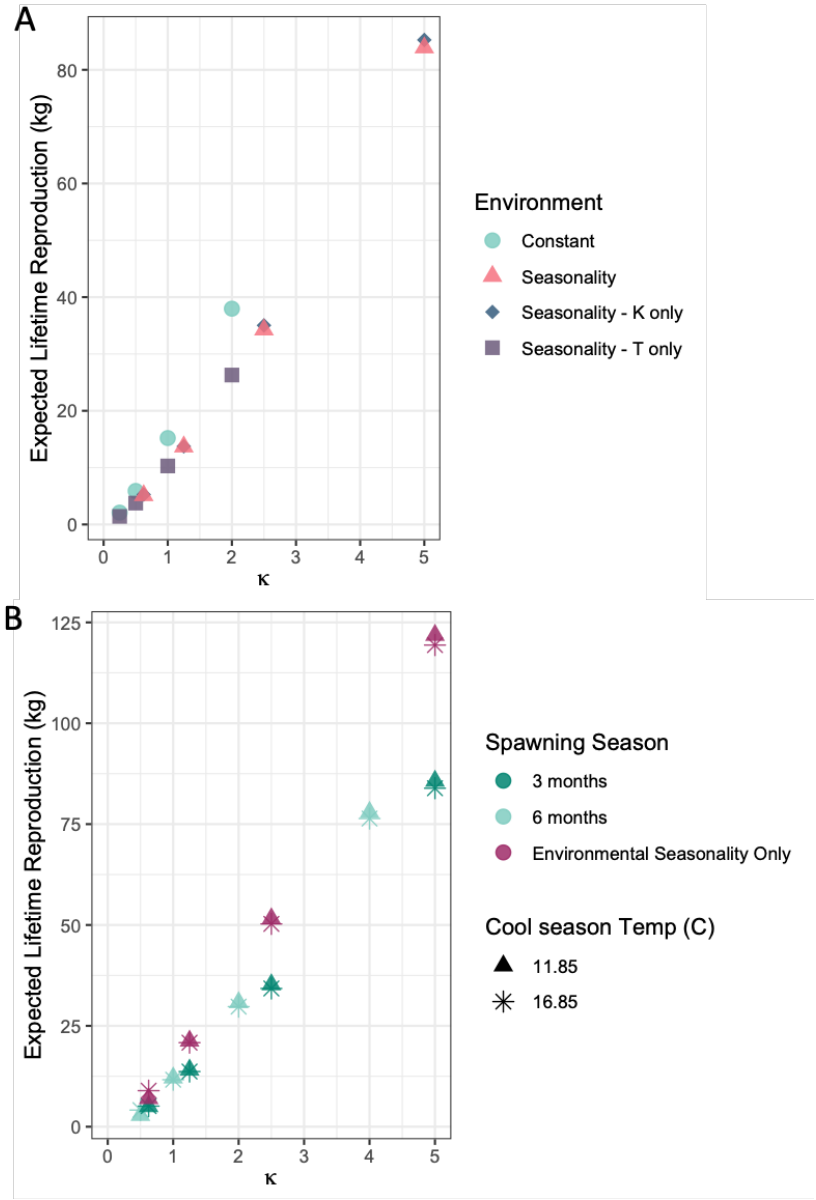

Supplementary Figure 10. Lifetime reproduction across values of κ and temperature in all scenarios of seasonality in food, temperature, and spawning season duration in Fig 7. Note that the darker teal stars in panel B (corresponding to a three-month spawning season and a winter temperature of 16.85°C) match the fully seasonal scenario (pink triangle) in panel A. Magenta points correspond to the scenario where individuals can spawn year-round but do experience warm, resource poor conditions for three months of the year.